ACOUSTIC REFLECTION FROM TEMPERATURE MICROSTRUCTURE

Jishi Xie
Marine Studies Centre
Department of Geology & Geophysics
University of Sydney

A thesis submitted for the degree of
Master of Science

December 1989

ABSTRACT

This thesis develops a numerical technique to predict the acoustic reflection from an arbitrary sound speed microstructure in the ocean (or a temperature microstructure in the fresh water). This numerical technique is able to reproduce the theoretical formulas for calculating the reflection coefficients of two analytically defined transition layers.

The 50 kHz acoustic reflection coefficients from the temperature microstructure measured in a fresh-water reservoir was predicted to be less than -90 dB and was found to be much weaker than the observed volume scattering which was due to the biological activities.

Table of Contents

1. INTRODUCTION

For the convenience of studying the propagation of underwater sound, the ocean has often been assumed to be horizontally layered and homogeneous. But as a matter of fact, the real ocean is far from that ideal. In the ocean, especially in the upper layer, there are various kinds of acoustic scatterers, such as marine organism, bubbles (both generated by breaking waves and ship activities), suspended particles and sea water temperature microstructure. When a sound wave is travelling in this inhomogeneous media, its energy will be scattered and absorbed. Different scatterers have different reflectivities and the same scatterer has a different scattering strength at different sound frequencies.

The above-mentioned scatterers are often found in the water media between sonars and the targets. They cause reverberation and attenuation of a sound wave. Thus understanding the acoustic properties of all these scatterers is important for designing and operating a sonar.

On the other hand, if we understand the acoustic properties of scatterers well, we can study the other properties of these scatterers by using acoustic equipment.

Before the 1970's nearly all the information on atmospheric microstructure came from scattering observations, and very little from direct sounding, whereas in the ocean all came from direct sounding and none from scattering experiments (Munk & Garrett, 1973).

By the end of the 1960's radar backscattering from clear air had been well understood (Hans Ottersten, 1969). The theory on the radar returns as backscattering from refractive index perturbations due to isotropic fine-scale turbulence had been well developed and was supported by experimental data.

Scientists adopted the similar theory on studying acoustic backscattering from oceanic microstructure.

Tatarski (1961) was the first to calculate the acoustic scattering cross section from isotropic refractive index fluctuations in the ocean.

Munk & Garrett (1973) presented the acoustic cross section from horizontally layered refractive index fluctuations as a function of the one-dimensional spectrum of the deviation from the mean of the refractive index, and the sonar wave length.

Attempts at measuring the acoustic scattering from temperature microstructure, especially from internal waves, have been made since the 1970's.

Proni & Apel (1975) reviewed the calculations of Tatarski (1961) and Munk & Garrett (1973) and pointed out that there should be a higher acoustic scattering cross section from layered fluctuations than from nonlayered fluctuations. They used a high-frequency (5- to 25-kHz) acoustic echosounder to observe internal waves and compared the acoustic data with simultaneous temperature data (using a towed thermistor). A high degree of correspondence between them has been found. However, the question

concerning which type of scatterer was contributing which part of the acoustic return remained.

Kaye (1978) found a correlation between acoustic scattering intensity at 87.5 kHz and small scale vertical temperature gradients. He suggested that the measured scatterers should not be considered as passive scalars of the temperature profile, even though they may serve as tracers of internal wave activity.

High-frequency (wave length ≈ 400m), near-surface internal wave groups in the deep ocean were said to be observed by Proni et al. (1978). The acoustic return was observed from a depth of 25m to a depth of about 70m, which was received by a 20kHz echosounder towed a few metres below the surface. The scattering strength of the internal wave groups observed was not mentioned. Since plankton tend to stay in a thermocline, it may be plankton that was scattering high frequency sound. It is uncertain that whether backscatter from the change of a thermocline alone is detectable (Clay & Medwin 1977).

Microstructure reflection at 8kHz was reported to be observed by Kaye & Anderson (1979). A large-aperture planar hydrophone array was used, which was able to discriminate against biological scatterers on the basis of wave front curvature. The reflections were highly directional, with response dropping in excess of 15 dB as the beam steering direction varied from normal incidence to 2° off normal. With an 87.5 kHz echosounder, microstructure reflections were not seen and most of the reverberation was found due to discrete point scatterers.

Since acoustic reflection from naturally occurring temperature microstructure was difficult to detect, attempts were made to measure scatter from artificially generated turbulence by some people. Thorpe and Brubaker (1983) discussed sound reflection from the wake of towed objects, which were two 25kg weights, tied together, hanging 12m below the ship. The acoustic returns from such weights were observed with a 102 kHz narrow-beam fisheries research transceiver sonar in a fresh water lake in western Australia.

Brekhovskikh (1980) determined the acoustic reflection coefficient of some particular velocity structure layers, e.g. the transition layer, symmetric layer and linear layer. But in nature there is no velocity microstructure shaped precisely like those mentioned above. Techniques for dealing with more realistic cases are needed.

Compared with the reflection from oceanic microstructure, the acoustic scattering from air bubbles in the water and marine organisms has been more often reported in the literature, probably because they are stronger scatterers.

Bubble clouds generated by breaking-waves near the sea surface cause a strong reverberation of mm-wave-length underwater sound. Detecting and studying bubble clouds by means of acoustics has been attempted by some people. Thorpe (1986) used an upward-looking, bottom-mounted sonar, a telesounder, and a dual-beam side-scan sonar to detect bubbles. He found that bubbles penetrate deeper as the wind speed increases, the probability distribution of M_v, the acoustic scattering cross section per

unit volume at constant depth, are close to logarithmic normal, and the value of M_v at same depth and same wind speed are greater in the sea than in the fresh-water loch. Fetch also appears to be an important variable.

Multichannel false colour echograms were sometimes used as a tool for biological interpretation in the ocean (Cochrane & Sameoto, 1986). 50 kHz and 200 kHz acoustic backscattering profiles were obtained and compared with direct multilevel net sampling data in the central Scotian Shelf. The results showed that strong 200 kHz scattering layers below 100 m depth were compatible with "Rayleigh" scattering from copepods, layers in the upper 60 m scattering with nearly equal strengths at 51 kHz and 200 kHz were ascribed to comparatively large fish scattering in "geometric" regime. (A "Rayleigh" scatterer is an object whose dimensions are much smaller than the wave-length of the incident sound. Its acoustic cross section increases as the fourth power of the sound frequency. A "geometric" scatterer is one whose dimensions are much larger than the wave-length of sound and its acoustic cross section is invariant with the sound frequency.)

Volume backscattering from plankton both in the ocean and lakes, which varies with sound frequency, time of day, and depth, has been investigated by many people. See Beamish (1971), Hall (1973), and Clay & Medwin (1977).

Suspended particles are considered to be very weak scatterers due to their small size and non-resonant behaviour, unless their density is very high, Proni et al., (1976).

This thesis reviews the previous research and results on acoustic scattering in the upper ocean, and presents some results on studying acoustic reflection from natural temperature microstructure and biological scatterers. A newly developed numerical technique for calculating reflection coefficient of temperature microstructure of any shape is described in Chapter 3. Then comparison is made between acoustic scattering from temperature structure and other scatterers in the upper ocean.

2. EXPERIMENTAL METHODS

2.1 Echosounder

An echosounder with a 50 kHz transducer, 9° of beam width and 1.632 ms of pulse duration, was used for measuring the acoustic backscattering in the upper layer of the water. It has a colour video display which presents the echo level as one of the eight colours each 5 dB apart in acoustic intensity.

The echosounder was calibrated with a standard hydrophone in order to determine the relation between the colours shown on the video display and the the echo level at the transducer.

The calibration of the echosounder is shown in Appendix A.

The echosounder was set to have constant gain with time where it had maximum detecting ability.

2.2 Measurement of Temperature Microstructure

PORPUS (Probe for Repeated Profiling of Upper-Ocean Stratification) was used to measure temperature microstructure in Woronora Dam, a fresh water reservoir in the south of Sydney on which DSTO (the Defence Science and Technology Organization) maintains a small pontoon. It was designed to resolve temperature fluctuations to better than 1 m°C over vertical scales of 0.7 to 3 cm in order to observe gravitationally unstable structures in the upper layer of oceans or lakes. A schematic of PORPUS is shown in Fig.2.1. The probe consists a streamlined body, a thermistor, three primary fins at the rear of the body to provide rotational inertia and increased drag to reduce the probe's terminal velocity. The fall rate was checked by means of tracking with an echosounder.

Data was sent to the surface via a teflon-coated co-axial cable which, with the thermistor, formed an arm of a bridge circuit. The output voltage from the bridge was digitised by an HP-3478a multimeter, then recorded via HP-IB interface onto an HP-85B microcomputer.

This device is described in more detail in Padman & Jones (1987).

An example of temperature microstructure measured by PORPUS and plotted out by an HP-85B microcomputer is shown in Fig.2.2. The data are then used to calculate the reflection coefficient of the temperature structure. This will be described in Chapter 3.

3. ACOUSTIC REFLECTION FROM A TEMPERATURE MICROSTRUCTURE

3.1. Introduction

Formulas of the reflection coefficient for a few simple forms of sound velocity structure have been reported previously, such as the 3 formulas presented in Brekhovskikh (1980). These are reproduced below.

Eq.3.11 is for the reflection coefficient of a transition layer (curve 1 in Fig.3.1). Eq.3.13 and Eq.3.14 are for a linear layer (curve 2 in Fig.3.1).

$$R = \frac{\sinh[\pi S/2(1-(1-N)^{\frac{1}{2}}]}{\sinh[\pi S/2(1+(1-N)^{\frac{1}{2}}]} \qquad (3.11)$$

where N is a constant defined by the maximum sound velocity difference of a transitional layer.

$S \equiv 2k_0/m$ is the relative thickness of the layer.

m is a constant related to the thickness of the layer.

k_0 is the wave number in the medium from which the sound is incident.

$$R = \frac{\sinh(\mu\ 1nn_1)}{[\sinh^2(\mu\ 1nn_1)+4\mu^2]^{\frac{1}{2}}} \qquad (3.13)$$

for $k_0 LA < 1/2$,

where $n_1 \equiv k/k_0$ is the index of refraction for $z \geq L/2$.

k is the wave number in the medium considered.

$\mu = [1/4-(k_0 LA)^2]^{\frac{1}{2}}$, L is the thickness of the layer. $A = n_1/(1 - n_1)$.

$$R = \frac{\sinh(w \ln n_1)}{[\sin^2(w \ln n_1)+4w^2]^{\frac{1}{2}}} \qquad (3.14)$$

for $k_0 La > 1/2$,

where $w = [(k_0 LA)^2 - 1/4]^{\frac{1}{2}}$.

The two sound velocity structures in Fig.3.1 are not likely to be found in nature. The naturally measured ones are completely irregular, see Fig.2.2, and their reflection coefficient can not be expressed with formulas like those mentioned above.

A numerical calculation technique has been developed to calculate the reflection coefficient from temperature microstructure of general form. The main idea is dividing a region of temperature gradient into a large number of thin layers such that each layer is thinner than the wave length of incident sound and adding both the amplitude and the phase of the reflection coefficient at each thin layer together, ignoring the multiple reflections (these will be discussed in Appendix B). The reflection coefficient becomes

$$R = \sum_{j=1}^{n} R_j \exp(-i2kjd) \qquad (3.15)$$

where R_n is the amplitude of the reflection coefficient of Number j layer.

k is the wave number.

d is the thickness of each thin layer.

Eq.3.15 can be only calculated with the aid of computer because reflections from thousands of thin layers are involved. Full details of this technique is described in the following three sections.

3.2 Numerical Calculation of The Reflection Coefficient for a Linear Layer

Consider a free plane wave, normal incident on a sound velocity structure in water (Fig.3.2). For the convenience of calculation, we make the following simplification: 1. water is an idea medium in which no energy loss will occur when a sound wave is travelling. 2. the water is a Newtonian fluid. 3. the water is macroscopically static. 4. the sound velocity structure in water is horizontally homogeneous.

The linear layer in Fig.3.2 is divided into a large number of thin layers with equal thickness δz such that each layer is much smaller than the wave length of incident sound. i.e. $\delta z \ll x$. Since the multiple reflections have been ignored, the reflection coefficient for sound pressure at the single step in position z is identical with the one when this step exists alone. i.e.

$$\delta V = (\beta_i C_i - \beta_{i-1} C_{i-1})/(\beta_i C_i + \beta_{i-1} C_{i-1}) \quad \ldots.(3.20)$$

where β is the density of the water.

C is the sound velocity.

Since there is no impurity in water, the assumption $\beta_i \approx \beta_{i-1}$ is reasonable.

If G is the gradient of the linear layer, we have

$$C_i = C_{i-1} + G\delta z$$

$$C_{i-1} = C_0 + Gz$$

where C_0 is the sound velocity at $z = 0$.

$G = \dfrac{C_D - C_0}{D}$ is the gradient of sound speed, in 1/s.

D is the thickness of the linear layer.

C_D is the sound speed at $z=D$.

Then we get

$$\delta V = (C_i - C_{i-1})/(C_i + C_{i-1})$$

$$= G\delta z/(2C_0 + 2Gz + G\delta z)$$

Considering the phase, which equals 0 at $z = 0$, the complex reflection coefficient is

$$\delta R = G\delta z \exp(-i2kz)/(2C_0 + 2Gz + G\delta z)$$

$$= \frac{G\delta z \exp(-i4\pi Fz/C)}{2C_0 + 2Gz + G\delta z}$$

$$= \frac{G \exp[-i4\pi Fz/(z + C_0/G)/G]}{2[C_0 + z(C_D - C_0)/D + G\delta z/2]} \delta z \qquad (3.21)$$

where F is the sound frequency.

We will show that since the change in speed of sound is small through the whole layer, $i2kz \approx i2k_0 z$

Since $|(C_D - C_0)/C_0| \ll 1$, $z \le D$ and $\delta z \ll D$, we have

$$\frac{(C_D - C_0)z}{D} \le (C_D - C_0)/2 \ll C_0$$

and $$G\delta z/2 \le GD/2 = C_D - C_0 \ll C_0$$

and $$z \le D \ll C_0/G$$

Eq.3.21 becomes

$$\delta R \approx \frac{G \exp(-i4\pi z/\lambda_o)}{2C_0} \delta z \qquad (3.22)$$

where λ_o is the wave length at z = 0.

when δz is approaching zero, we have

$$dR = \frac{G \exp(-i4\pi z/\lambda_o)}{2C_0} dz \qquad (3.23)$$

taking the integral of Eq.3.23, we get the reflection coefficient of the linear layer,

$$R = \int_0^D dR = \frac{G}{4\pi F} \sin(\frac{2\pi D}{\lambda_o}) \exp(-i2\pi d/\lambda_o) \qquad (3.24)$$

where F is the sound frequency.

Eq.3.24 shows the reflection coefficient for sound pressure. The square of R'is the reflection coefficient for sound intensity,

$$R^2 = R\ R^* = (\frac{G}{4\pi F} \sin \frac{2\pi D}{\lambda_o})^2 \qquad (3.25)$$

Fig.3.3 shows the changes of the reflection coefficient R^2 as a function of the thickness of the layer.

3.3. The Reflection Coefficient of Arbitrary Profiles

Consider a sound velocity microstructure layer such as that in Fig.2.2. Firstly we divide the layer into n small thin layers with equal thickness d (hereunder we refer to d as " the numerical step size" or "sampling separation"). n must be large enough that the numerical step size d meets the following two requirements (The reason will be given in Appendix C. See also Section 3.6):

(1). $d \leq \lambda_o/4$, where λ_o is the incident sound wave length.

(2). $d \ll h$, where h is the thickness of the fluctuation with the smallest vertical scale in the sound velocity microstructure such that the change of sound velocity in each thin layer is approximately linear.

Now we have

$$G_j = \text{constant}$$

where G_j is the sound velocity gradient of Number j small layer, which is defined as $(C_j - C_{j-1})/d$,

where C_j is the sound velocity at the top side of Number j layer, C_{j-1} is the sound velocity at the bottom side of Number j layer, d is the thickness of Number j layer.

by using Eq.3.23, the expression for a small region within the thin layer J, we can get the reflection coefficient of Number j layer

$$R_j = \int_{z_{j-1}}^{z_j} \frac{G_j \exp(-i2k_0 z)}{2C_0}\, dz$$

$$= \frac{ix_0 G_j \exp(-i2k_0 z)}{8\pi C_0}\Bigg|_{z_{j-1}}^{z_j}$$

$$= \frac{G_j}{8\pi F}[(\sin 2k_0 z_j - \sin 2k_0 z_{j-1}) + i(\cos 2k_0 z_j - \cos 2k_0 z_{j-1})] \qquad (3.31)$$

where $F = C_0 / \lambda_0$ is the frequency of the incident sound.

$k_0 = 2\pi / \lambda_0$ is the wave number at $z = 0$.

$z_j = jd$ is the depth of Number j layer, where d is the thickness of Number j layer.

$z_{j-1} = (j-1)d$.

or

$$R_j = \frac{G_j}{8\pi F}\{\sin 2k_0 jd - \sin 2k_0 (j-1)d + i[\cos 2k_0 jd - \cos 2k_0 (j-1)d]\}$$

$$= \frac{\sin k_0 d}{4\pi F} G_j [\cos k_0 d(2j-1) - i \sin k_0 d(2j-1)] \qquad (3.32)$$

or

$$R_j = \frac{G_j \sin k_0 d}{4\pi F} \exp[-ik_0 (2j-1)d]$$

where $\frac{G_j \sin k_0 d}{4\pi F}$ is the modulus of the reflection coefficient in Number j layer, while $\exp[-ik_0(2j-1)]$ is the phase.

By adding up the reflection coefficient, including the moduluses and the phases, of all n layers (because the acoustic pressure of the reflections can be added), we can get the reflection coefficient of the whole sound velocity microstructure (see Appendix B):

$$R = \sum_{j=1}^{n} R_j = \frac{1}{4\pi F} \sum_{j=1}^{n} G_j \sin(k_0 d)[\cos k_0(2j-1)d - i \sin k_0(2j-1)d] \qquad (3.33)$$

3.4. The Reflection Coefficient of Two Transitional Layers and the Comparison with Theoretical Results

3.4.1. A Linear Layer

We wish to compare the numerical technique with the known analytical solution for particular profiles.

The sound velocity profile to be considered is shown in Curve 2, Fig.3.1.

Fig.3.3 shows the reflection coefficient of the linear layer calculated with numerical technique, Eq3.33, which is compared with the theoretical result from Eq.3.14. They match closely.

As a matter of fact, under some conditions Eq.3.14, the theoretical formula of the reflection coefficient at a linear layer, can be simplified as Eq.3.25, the limit of the numerical formula for calculating the reflection coefficient of a linear layer. This will be proved in the following.

There are two formulas, Eq.3.13 and Eq.3.14, for the linear layer under two different cases, (1) $k_0 LA < 1/2$; (2) $K_0 LA > 1/2$. We will choose Eq.3.14 to discuss because, in the water of oceans or lakes, case 2 is always appropriate when sound of not very low frequency is considered. This is described bellow:

Because the index of refraction for $z \geq L/2$

$$n_1 = k_1/k_0 = C_0/C_1$$

we get

$$A = \frac{n_1}{1-n_1} = \frac{C_0}{C_1 - C_0}$$

and the gradient of sound velocity

$$G = (C_1 - C_0)/L$$

so we have

$$k_0 LA = \frac{2\pi F L C_0}{C_0 (C_1 - C_0)}$$

$$= \frac{2\pi F}{G}$$

then for $k_0 LA >> 1$, $G << 2\pi F$.

Since G is never larger than 100 (1/s) in the water, if the frequency of sound used is much higher than $G/2\pi$, $k_0 LA >> 1$ is tenable. Then we can make the following simplification,

$$w = [(k_0 LA)^2 - 1/4]^{\frac{1}{2}}$$

$$\approx k_0 LA$$

$$= \frac{2\pi F}{G}$$

Eq.3.14 becomes

$$R = \frac{\sin(w\ 1nn_1)}{[\sin^2(w\ 1nn_1)+4w^2]^{\frac{1}{2}}}$$

$$\approx \frac{\sin(k_0 LA\ 1nn_1)}{[\sin^2(k_0 LA\ 1nn_1)+4(k_0 LA)^2]^{\frac{1}{2}}}$$

$$\approx \frac{\sin(k_0 LA\ 1nn_1)}{2k_0 LA}$$

$$= \frac{\sin\left[\frac{k_0 LC_0\ \ln(C_0/C_1)}{C_1 - C_0}\right]}{4\pi F/G}$$

$$= \frac{\sin\left[-k_0 LC_0 \frac{\ln(1+\delta C/C_0)}{\delta C}\right]}{4\pi F/G}$$

where $\delta C = C_1 - C_0$.

If $|\delta C/C_0| << 1$ is satisfied, we have,

$$\ln(1+\delta C/C_0) \approx \delta C/C_0$$

then the reflection coefficient

$$R = \frac{\sin(-k_0 L)}{4\pi F/G}$$

$$= \frac{-G\sin(k_0 L)}{4\pi F}$$

and

$$R\ R^* = \left[\frac{G\sin(k_0 L)}{4\pi F}\right]^2$$

which is the same as Eq.3.25, where L = D is the thickness of the layer.

3.4.2. A Transitional Layer

Curve 1 in Fig.3.1 shows the sound velocity profile of a transitional layer.

Fig.3.4 is a set of comparisons between numerical results and theoretical results when the thickness of the transitional layer increases. We can see that, when the the numerical step size d is not much smaller than the wave length λ_o, i.e.

$$\lambda_o/d < 4$$

there is a large error in all 6 cases in Fig.3.4.

When $\lambda_o/d > 4$

we observe good match between the numerical and theoretical results in (c), (d) and (f) in Fig.3.4 (See also Appendix C). Errors occuring in (a) and (b) are due to the limit of the precision of the computation while that in (f) is because the thickness of the transitional layer is too small (compared with the acoustic wave length) i.e.

$$k_0 h < 1$$

The second requirement is not satisfied (Here the thickness of the transitional layer, h, is "the smallest vertical scale of sound velocity fluctuation")

Details will be discussed in Section 3.6.

3.5. Acoustic Reflection Coefficient of Measured Temperature Microstructure

3.51. Measured Temperature Microstructure

In fresh water the sound velocity is a function of temperature and water pressure (Clay & Medwin 1977):

$$C = 1402.3+4.95T-0.055T^2+0.00029T^3+0.016z \quad (3.51)$$

where C is the sound velocity, m/s.
T is the water temperature, °C.
z is the depth of water, m.

With the aid of Eq.3.51 we can transfer the data of temperature microstructure, measured with PORPUS probe which is described in Chapter 2, into sound velocity. Then we can use Eq.3.33 to calculate the reflection coefficient of such a structure.

Firstly we should examine if the data collected with the PORPUS probe meet the two requirements when using Eq.3.33. i.e.

(1). the numerical step size must not be larger than the 4th of the acoustic wave length.

(2). the numerical step size must be much smaller than the smallest vertical scale of the step in the sound velocity microstructure.

The fall speed of the PORPUS probe is adjustable, ranging from 22cm/s to 40cm/s while the sampling separation d (this means over every d cm in the vertical scale a temperature value is recorded) changes from 0.7097cm to 3cm.

If we choose sampling density of d = 0.7097cm, we have better depth resolution.

Fig.2.2 is a temperature microstructure measured with PORPUS probe in Woronora Dam in 25/5/1989. The fall speed of the probe was 0.22m/s. The vertical interval was 0.7097cm. If acoustic reflection for 50kHz is required, the acoustic wave length λ_o= C/F, where C is the sound velocity of water, which is around 1480m/s, F is the frequency. Then λ_o = 2.96cm. Thus the requirement $d \leq \lambda_o/4$ is satisfied.

We also have to find out whether the second requirement $d \ll h$ is met.

A temperature microstructure can be seperated into two parts: the smooth mean profile and the fluctuating part whose distribution of energy is determined with the so-call temperature-gradient spectrum. Kolmogorov (1941) proposed that all turbulent velocity spectra are reducible to a single universal curve for the highest wave-numbers and that, under certain conditions, dimensional analysis may be used to predict spectral shapes. Identical arguments predict that the fine structure of conserved dynamically passive scalar fields mixed by turbulence will also be universal similar (See Gibson & Schwarz, 1963). Batchelor (1959) determined the form of the temperature spectrum for

higher wave numbers where viscous and diffusive effects are important (See Newberger & Caldwell, 1981).

According to Batchelor's temperature spectrum (Gibson & Schwarz, 1963), the perturbation of temperature approaches to zero rapidly when the wave length of its Fourier component is very small. If we can prove that when the vertical scale is smaller than the depth resolution of PORPUS, the temperature fluctuations are so little that they can be ignored, then we can say the second requirement of the numerical technique is fully satisfied.

The one dimensional Batchelor spectrum for temperature gradient can be written as (Newberger & Caldwell, 1981)

$$S(k) = (\pi q)^{\frac{1}{2}} \chi (k_B D)^{-1} f[(2q)^{\frac{1}{2}} k/k_B] \qquad (3.52)$$

where q is a universal constant,

k_B is the Batchelor wave number, $k_B = (\epsilon v^{-1} D^{-2})^{\frac{1}{4}}$,

ϵ is the dissipation rate for kinetic energy,

v is the kinematic viscosity,

D is the thermal diffusivity,

χ is the dissipation rate for temperature variance satisfying

$$\chi = 6D\int_0^\infty S(k)dk = 6D\overline{\left(\frac{dT}{dz}\right)^2}$$

the universal function is given by

$$f(y) = (2\pi)^{-\frac{1}{2}} y[\exp(-\tfrac{1}{2}y^2) - y\int_y^\infty \exp(-\tfrac{1}{2}t^2)dt]$$

$$= (2\pi)^{-\frac{1}{2}} y\exp(-\tfrac{1}{2}y^2) - \tfrac{1}{2}y^2 \operatorname{erfc}(y/\sqrt{2}) \qquad (3.53)$$

The spectrum is shown in Fig.3.5.

When the wave length $\lambda \to 0$, or $y \to \infty$, $f(y) \to 0$.

The average of square root of the gradient of temperature fluctuation (hereunder we refer to it as "average fluctuation gradient") for those short wave-length components, $k \geq k_a$, can be calculated from

$$\overline{\left(\frac{dT}{dz}\right)^2} = \int_{k_a}^{\infty} S(k)\,dk$$
$$= \chi(6D)^{-1}\left[(\pi/2)^{\frac{1}{2}} y^3 \operatorname{erfc}(y/\sqrt{2}) + (1-y^2)\exp(-\tfrac{1}{2}y^2)\right] \qquad (3.54)$$

where $y = 2\pi(2q)^{\frac{1}{2}}/\lambda_a/k_B$

We assume that a temperature fluctuation component with a wave length λ is equivalent to a temperature step whose vertical scale is equal to $\lambda/4$ in the temperature microstructure. See Fig.3.6.

To calculate the average fluctuation gradient for those perturbations whose vertical scales are smaller than 0.7097cm, we just calculate that for those components whose wave length $\lambda \leq 4*0.7097\text{cm} = 2.84\text{cm}$.

We choose the values of the relevant factors as below (High values of ϵ and χ and low value of q are chosen to enable that S(k) reaches its high value extreme for a given high wave number, or small wave length, in the range when $y>1$, for the following discussion is within this range. Thus if the following conclusion

under this high value extreme is correct, it will be also valid when the average or low values of ϵ and χ, and the average or high value of q are chosen.):

$$\epsilon = 10^{-2}\ cm^2/s^3,$$

$$D = 0.19\ cm^2/s,$$

$$v = 0.14\ cm^2/s,$$

$$q = 2.4,$$

$$\chi = 10^{-4}\ ^\circ C^2/s.$$

Applying Eq.3.54, we get the average fluctuation gradient for $\lambda \le 2.84\ cm$

$$\sqrt{\left[\frac{dT}{dz}\right]^2}\ \Bigg|_{\lambda \le 2.84\ cm} = 5.86*10^{-5}\ ^\circ C/cm$$

while the average fluctuation gradient for all wave length is

$$\sqrt{\left[\frac{dT}{dz}\right]^2}\ \Bigg|_{0 \le \lambda \le \infty} = (\chi/6/D)^{\frac{1}{2}} = 9.4*10^{-3}\ ^\circ C/cm$$

and

$$\frac{\sqrt{\left[\frac{dT}{dz}\right]^2}\ \Big|_{0 \le \lambda \le \infty}}{\sqrt{\left[\frac{dT}{dz}\right]^2}\ \Big|_{\lambda \le 2.84}} \approx 160$$

From Eq.3.33 we know that the reflection coefficient is

proportional to the gradient of the sound speed which is proportional to the temperature gradient in the fresh water. So the reflection coefficient is

$$R \in 10\log\left(\frac{dC}{dz}\right)^2 \in 10\log\left(\frac{dT}{dz}\right)^2 = 20\log\left(\frac{dT}{dz}\right)$$

then the difference between the reflection coefficient of the average fluctuation gradient for those wave length $0 \leq \lambda \leq \infty$ and for those $\lambda \leq 2.84$ is

$$\delta R = R_{0 \leq \lambda \leq \infty} - R_{\lambda \leq 2.84} = 20\log(160) = 44\text{dB}$$

The above analysis suggests that the depth resolution of PORPUS is sufficient for measuring the significant fluctuations in the temperature microstructure. The second requirement for calculating the reflection coefficient of a temperature microstructure can be satisfied.

3.52. The Acoustic Reflection from a Measured Temperature Microstructure

We wish to predict the reflction from the temperature depth measurements with a sound pulse length of τ (ms) at 50 kHz in Woronora Dam.

When a PORPUS probe is falling vertically through the water, a temperature value is read every d unit in depth. See Fig.3.8.

We divide this structure into n layers with equal thickness d. At number j layer the temperature difference is $T_j - T_{j-1}$. According to Eq.3.51 we get

$$G_j = \left.\frac{dC}{dz}\right|_{z=jd} = \frac{\partial C}{\partial T}\frac{dT}{dz} + \left.\frac{\partial C}{\partial z}\right|_{z=jd}$$

$$= (4.95 - 0.11T_j + 0.00087T_j^2)\left.\frac{dT}{dz}\right|_{z=jd} + 0.016$$

Because temperature gradient $\left.\frac{dT}{dz}\right|_{z=jd}$ is $(T_j - T_{j-1})/d$, so

$$G_j = (4.95 - 0.11T_j + 0.00087T_j^2)(T_j - T_{j-1})/d$$

$$+ 0.016 \qquad (3.55)$$

Using Eq.3.33 and substituting Eq.3.55, we get the reflection coefficient from part of this temperature structure ("part of it" means n thin layers of the total structure, the thickness of each thin layer is d.)

$$R = \frac{1}{4\pi F} \sum_{j=1}^{n} \sin(k_0 d)[(4.95-0.11T_j+0.00087T_j^2)$$

$$(T_j-T_{j-1})/d+0.016][\cos k_0(2j-1)d - i\sin k_0(2j-1)d] \quad \ldots\ldots (3.56)$$

where k_0 is the wave number in the medium where sound is incident.

d is sampling separation, m,

F is the sound frequency, Hz,

T_j is the water temperature at the bottom side of Number j layer, °C,

n, the total number of thin layers, is determined by the pulse length of the echosounder L and d,

$$L = C\tau$$

where C is the sound velocity, m/s,

τ is the pulse duration, s.

As shown in Fig.3.9, the thickness D, which contains n thin layers of reflector, is such that, with a pulsed echosounder, the reflection produced by all n layers arrives back at the receiver at the same time. When a sound pulse is incident on these n layers, the reflection wave of the front end of the pulse by Number n layer at r_2 will arrive back at the receiver at the same instant as the reflection wave of the rear end of the pulse by Number 1 layer at r_1. D must accordingly be $L/2 = C\tau/2$.

So we have

$$n = D/d = C\tau/2/d$$

where d is the numerical step size or the sampling separation.

The pulse duration of the echosounder used in Woronora Dam was 1.632 ms. So D=L/2=1480×1.632×0.001/2=1.20768 m. If the sampling separation d = 0.007097m, then

$$n = D/d = 170$$

The calculation of Eq.3.56 was completed with an HP-85 microcomputer, which plotted the reflection coefficient against depth from the temperature structure shown in Fig.2.2 when the sound pulse was travelling through it. The accuracy of the computer is $10^{(-11)}$.

Each point at a depth of z in Fig.3.7 represents the reflection coefficient from the temperature structure at a depth of from z to z + $C\tau/2$ that contains n layers. Since the sampling separation for measuring temperature microstructure on the three dates shown in Fig.3.7, d=0.7097 cm, the two requirements for the calculation of 50 kHz acoustic reflection from those three microstructure are satisfied (see discussion on Section 3.51).

3.6. The Error of the Numerical Calculation Technique

When using Eq.3.56 to calculate the reflection coefficient from a temperature microstructure, if the two requirements of Section 3.3 are not met, or the temperature probe for measuring temperature microstructure has not enough resolution, or the computer precision is not high enough, errors will occur.

The following analysis is based on a series of plots of reflection coefficient from a transitional layer versus different λ_o/d, where λ_o is the sound wave length and d is the numerical step size (Fig.3.4). These figures reveal three causes of the errors.

3.6.1. Error Occuring When $\lambda_o/d < 4$

Let us consider a case where the acoustic wave length is not small compared with the numerical step size.

Consider a transitional layer with small change of sound velocity, which is expressed as

$$C = C_1 \sqrt{\frac{1+\exp(mz)}{1+\exp(mz)-N\exp(mz)}} \qquad (3.61)$$

where m = 3.52/h, is a constant. h is the thickness of the layer,

$$N = (C_1^2 - C_2^2)/C_2^2$$

N determines the total change of sound velocity in the layer. we choose N = 0.001.

$$\frac{dC}{dz} = \frac{C_1 m N e^{mz}}{2(1+e^{mz})} \cdot \frac{1}{(1-\frac{Ne^{mz}}{1-e^{mz}})^{\frac{1}{2}}} \qquad (3.62)$$

because $N \ll 1$, $\frac{Ne^{mz}}{1+e^{mz}} \ll 1$

we can approximate Eq.3.62 by a series,

$$\frac{dC}{dz} \approx \frac{C_1 m N e^{mz}}{2(1+e^{mz})^{\frac{1}{2}}} \qquad (3.63)$$

substituting Eq.3.63 as the gradient at depth of z in Eq.3.33, we get the reflection coefficient of the transitional layer,

$$R = \frac{C_1 N m}{8\pi F} \sum_{j=1}^{n} \frac{e^{mz}}{(1+e^{mz})} \sin(k_0 d)[\cos k_0 d(2j-1) - i\sin k_0 d(2j-1)] \qquad (3.64)$$

If $d > \lambda_0/4$, there will be less than two samples per cycle in a sine (and cosine) component. See Appendix C. Error will occur, as illustrated in Fig.3.10.

3.6.2. Error Occuring When d > h

If the numerical step size d is larger than that of the transitional layer h, in other words, to replace a transitional layer with a linear layer whose thickness is larger (than that of the transitional layer, see Fig.3.11), one can not expect the reflection of the two layers will be close to each other because the two different profiles are not close at all. Here is an example when the thickness of the transitional layer, h, is smaller than the sampling separation, d, the numerically calculated reflection coefficient of the transitional layer will match the analytically calculated one (see Fig.3.12).

The thickness of the transitional layer is

$$h = 3.52/m = 0.07\text{cm}$$

and for a 50kHz sound wave, the wave length

$$\lambda_o = 2.96\text{cm}$$

We will discuss how the error of the numerically calculated reflection coefficient of the transitional layer changes from the case when $d \gg h$ to that when $d \ll h$: In Fig.3.12 we can see when $d > h$ (or $\lambda_o/d < 41$), there is a big error of the numerical result in this λ_o/d range. Even when $1 \leq h/d < 1.4$ (or $41 \leq \lambda_o/d < 58$), there is still a small error. Only when $d \ll h$ (or $\lambda_o/d > 58$), do the numerical result matches the theoretical result well. See also 2 in Appendix C.

If we take this transitional layer to be the the fluctuation with the smallest vertical scale in the sound velocity microstructure,

we can see why the second requirement in Section 3.3 is essential to the numerical technique for calculating the reflection coefficient of a sound velocity microstructure.

3.6.3. Error Caused by the Computer

The precision of computer may limit the accuracy of the numerical technique because the acoustic reflection coefficient is usually very small and that it might be beyond the precision of the computer.

Fig.3.13 is a plot of reflection coefficient when the thickness of the transitional layer h, is 9.8cm and the acoustic wavelength λ_o is 2.96cm (we assume that the speed of sound of the medium where $z = -\infty$, $C_0 = 1480$ m/s and the frequency of incident sound F = 50 kHz). The change of sound speed of the transitional layer is 0.726 m/s. Such a layer has a reflection coefficient of -362.8dB, or 7.08 E^{-19}, which is beyond the precision of the computer used for the numerical calculation. This does not happen when the reflection coefficient of the layer is not so small, see (c), (d), and (e) in Fig.3.4.

When $\lambda_o/d > 4$, $d < 0.74$cm. The requirements

$$d \ll h$$

and

$$d \leq \lambda_o/4$$

are satisfied. But there is still a large error between the numerical and the theoretical results. The reflection coefficient which was numerically calculated stays around -290 dB. This is because of the limit of the precision of HP-85 which was used for doing the numerical calculation.

The computer has a precision with a mantissa of 12 digits.

When $|mz| \leq 2$, the value of $\frac{e^{mz}}{(1+e^{mz})^2}$ in Eq.3.64, the reflection coefficient of a transitional layer, ranges from 0.1 to 0.25, see Fig.3.14, and the computing error is

$$E = 10^{-12}$$

The error of the reflection coefficient is approximately (See also Eq.3.64)

$$\delta R = \frac{C_1 N m \sin(k_0 d)}{8\pi F} E \qquad (3.65)$$

when $\lambda_o/d >> 1$, $\sin(k_0 d) \approx k_0 d = 2\pi d/\lambda_o$. Eq.3.55. becomes

$$\delta R = \frac{Nmd}{4} E \approx d \times 10^{-16}$$

Since there are n thin layers involved, if we do not consider the phase component, $[\cos k_0 d(2j-1) - i \sin k_0 d(2j-1)]$, the total error of the reflection ceofficient is estimated as

$$\begin{aligned} 20\log(\Sigma\delta R) &= 20\log(nd \times 10^{-16}) \\ &= 20\log(h \times 10^{-16}) \\ &\approx -300 \text{ (dB)} \end{aligned}$$

Using double precision will double the accuracy. An example is shown in Table 4 of the reflection coefficient of a transitional layer (when N=0.001, m=0.36) calculated by the numerical technique.

Precision of computer	Reflection coefficient
32 bits (real*4)	-220dB
64 bits (double precision)	-362.5dB

* The theoretical result is -362.8dB.

Table 4.Double precision makes the result of the numerical calculation more accurate.

In examples such as those in Fig.3.7 the calculated reflection is much greater than -220 dB. Thus not only the two requirements for using this numerical technique but the precision of the computer used were satisfied.

4. THE TYPICAL ACOUSTIC SCATTERING IN THE UPPER WATER

4.1 Introduction

50 kHz acoustic scattering in the upper layer of the oceans and lakes has seldom been reported in the literature. However, the few references all suggest that the biological scattering dominates over the upper ocean scattering.

Cochrane & Sameoto (1986) compared 51 kHz and 200 kHz acoustic backscattering profiles with direct multilevel net sampling data, showing that the scattering above 60 m was from fish and the scattering at a depth between 100 m and 250 m was from copepods. The scattering strength ranged from -60 dB to -90 dB.

To the best of our knowledge, no 50 kHz reflection from temperature microstructure has been reported.

At other frequencies, acoustic scattering from internal waves and microstructure was reported to be observed by some authors (Proni & Apel 1975, Kaye 1978, Proni et. al. 1978). But the cause of the scattering remained uncertain because of the biological masking.

A successful measurement that has been reported, of the acoustic reflection from natural microstructure alone, was made by Kaye & Anderson (1979) at 8 kHz. Their unique technique enabled the discrimination between reflectors and discrete point

scatterers. The high directivity of the microstructure reflection they have observed might suggest that layered microstructure is composed of sheet reflectors. And the fact that the microstructure had not been seen with a 87.5 kHz echosounder might suggest that the microstructure reflection was inversely proportional to the incident sound frequency (at least within this particular frequency range).

For the last two years, we have been trying to measure the acoustic reflection from the temperature microstructure with a 50 kHz echosounder in Woronora Dam. However, we found that the acoustic returns were dominated by volume scattering with a scattering strength of more than -85 dB, which did not correlate with the simultaneous temperature profile and was non-directional. The volume scattering was considered to be from biological organisms. The reflection from temperature structure predicted was much weaker.

4.2. Woronora Experiments

Over 20 measurements of acoustic backscattering at 50 kHz have been made in Woronora Dam since 1986. The water depth in the centre of this freshwater reservoir is about 56 m.

Twelve scattering experiments representing 4 different seasons (see Table 5) were averaged and the typical acoustic scattering profile in Woronora Dam is shown in Fig. 4.1. The acoustic backscattering strength is defined as

$$S = 1\log\left(\frac{I_s}{I_i}\right)$$

where I_s is the scattering intensity of a unit volume measured one metre from the equivalent acoustic centre of the scatterer,

I_i is the incident intensity also measured at the same place.

The two summer profiles were averaged and the variance of the results is shown as bars in Fig.4.2.

Spring	Summer	Autumn	Winter
30/10/87	4/11/87	9/4/86	13/7/87
8/8/88	6/12/88	10/2/88	13/5/88
		26/2/88	13/7/88
		14/4/88	
		14/4/88	

Table 5. Dates when acoustic data were collected in Woronora Dam.

Three temperature microstructure profiles were obtained with PORPUS probe on 8/8/88, 6/12/88 and 25/5/89. The temperature gradient in summer is normally larger than in winter. The average acoustic scattering is compared with temperature gradient, however, no correlation has been found (see Fig.4.2). Simultaneously measured acoustic scattering is then compared with temperature microstructure both in summer and winter (see Fig.4.3). The scattering profile does not follow the rhythm of the microstructure. No visual correlation is evident between them. It is clear that the acoustic scattering measured in Woronora Dam was not from temperature microstructure.

On two occasions, net sampling was taken in Woronora Dam. The results showed that the average concentration of copepods was up to several hundreds per cubic metre in the layers of top 20 m. This suggested that biological activities are the cause of the dominant 50 kHz acoustic volume scattering in this freshwater reservoir.

Compared with biological scatterers, the acoustic reflection from temperature microstructure is a weak reflector. The predicted reflection coefficient from microstructure is less than -90 dB both in summer and in winter while measured acoustic scattering exceeded -60 dB (see Fig.3.7, Fig.4.1, Fig.4.2 and Fig.4.3). The acoustic returns from temperature microstructure would be certainly "drowned out" by the biological scattering.

4.3 Discussion

The backscatter calculation assumes the vertical gradient of temperature is much larger than the horizontal. As this is a very reasonable assumption we must conclude that since our calculated levels of back-reflection are much less than that observed, the dominant scatter in this fresh water reservoir is not microstructure. It is difficult to imagine that sediments in suspension play an important role in acoustic backscatter from the upper water when there has not been recent significant runoff. The difference between the measured reflections and those calculated was large on all occasions investigated. We conclude that the dominant scatter must be biological in character.

It is suggested that further experiments to apply this numerical technique be carried out (1). in the "clean water" without volume scatterers but with high value of χ (the dissipation rate for temperature variance) so that large microstructure reflection can be delected alone; (2). using very low threshold echosounder that is able to measure weak reflection from temperature structure; (3). with lower frequency of sound to obtain stronger reflection.

5. CONCLUSION

This thesis develops a numerical technique to predict the acoustic reflection from an arbitrary sound speed microstructure in the ocean (or a temperature microstructure in the fresh water).

The ocean is often considered to be horizontally homogeneous. When any part of the vertical sound speed structure of interest is divided into a large number of thin layers and the thickness of each thin layer d satisfies 2 requirements: (1). $d \leq \lambda_o/4$, λ_o is the wave length of the sound used for detecting, (2), $d << \lambda_{max}$, λ_{max} is the wave length of the most energetic Fourier component of the sound speed structure, each of these thin layers can be treated as a linear sound speed layer. By adding up the reflection coefficient of each thin layer, we can get the total reflection coefficient of that part of sound speed structure.

This numerical technique is able to reproduce the theoretical formulas for calculating the reflection coefficient of two analytically described transitional layers.

An attempt to verify this numerical technique by experiments were made. The temperature microstructure was measured with PORPUS

Woronora Dam. The numerical technique was used to predict the acoustic reflection from those temperature structure. But the results showed that the reflection was too weak to explain the observations. Even the strongest reflection at 50 kHz (with a

reflection coefficient of -90 dB) from the temperature thermocline was below the threshold of the echosounder. Conversely the scattering from the volume scatterers either biological ones or air bubbles in the upper layer of the water was much stronger (the scattering strength measured was ranging from -40 dB to -80 dB).

ACKNOWLEDGEMENTS

First and foremost I would like to express my gratitude to my supervisor, Dr. Ian Jones, for his motivational guidance and constant supervision in the preparation of this thesis. His patience and his kind help to me in overcoming the difficulties I faced both in finance and in my research have been invaluable.

I deeply appreciate my wife, Bo Xu, for her wonderful encouragement and concern, especially during the last few months when I was completing this thesis.

The helpful support and assistance from Frank De Francisco, Jim Johnson and Bill Martin, D.S.T.O., and Mark Groskops, Dept. of Geology & Geophysics, University of Sydney, is much appreciated.

REFERENCES

Batchelor, G.K., 1959: Small Scale Variation of Convected Quantities Like Temperature Turbulent Fluid. J. Fluid Mech., 5, pp. 113-133.

Beamish, P, 1971: Quantitative Measurements os Acoustic Scattering from Zooplanktonic Organisms. Deep-sea Research, 1971, vol. 18, pp. 181-182.

Bendat, J.S. & Piersol, A.G., 1971: Random Data: Analysis and Measurement procedures. Wiley-Interscience. NY. p. 229.

Brekhovskikh, L.M., 1980: Wave in Layered Media. Academic Press NY, pp 503.

Clay, C.S. & Medwin, H., 1977: Acoustical Oceanography. John Wiley, NY, pp. 544.

Cochrane, N.A., & Sameoto, D.D., 1986: Multichannel False Colour Echograms as a Biological Interpretative Tool. Proc. 12th International congr. on Acoust. Associat. Symp. on Underwater Acoust. July pp. 16-18, 1986.

Gibson, C.H. & Schwarz, W.H., 1963: The Universal Equilibrium Spectra of Turbulent Velocity and Scalar Fields. J. Fluid Mech., 16, pp. 365-384.

Hall, M., 1973: Volume Backscattering in the Tasman Sea, the

Coral Sea, and the Indian Ocean. J. Acoust. Soc. Am. Vol. 54, No.2, pp. 473-477.

Kaye, G.T., 1978: Correlation between Acoustic Scattering and Temperature Gradient. J. Marine Res. 37, 2, 1978, pp. 319-326.

Kaye, G.T. & Anderson, V.C., 1979: Scattering From Oceanic Microstructure: Detection with Large Aperture Array. J. Acoust. Soc. Am. 66, 3.

Kolmogorov, A.N., 1941: The Local Structure of Turbulence. Dok. ANSSSR, 30, 301.

Munk, W.H., & Garrett, C., 1973: Internal Wave Breaking and Microstructure (The Chicken and The Egg). Boundry-layer Meteorol., 4, 1973, pp. 37-42.

Newberger, P.A. & Caldwell, D.R., 1981: An Internal Subrange in Microstructure Spectrua. J. Geophys. Res., 86, C5, 1981, pp. 4265-4268.

Ottersten, H., 1969: Radar Backscattering from the Turbulent Clear Atmosphere. Radio Science, Vol. 4, No. 12, pp. 1251-1255.

Padman, L. & Jones, I.S.F., 1987: Turbulence and Time-dependent Richardson Number. Stratified Flow. in press.

Proni, J.R. & Apel, J.R., 1975: On the Use of High-frequency Acoustics for the Study of Internal Waves and Microstructure. J. Geophys. Res., Vol. 80, No.9, 1975, pp. 1147-1151.

Proni, J.R., Newman, F.G., Sellers, R.L., & Parker, C., 1976: Acoustic Tracking of Ocean-Dumped Sewage Sludge. Science, 10 Sept. 1976, vol. 193, pp. 1005-1007.

Proni, J.R., Ostapoff, F., & Sellers, R.L., 1978: Acoustic Observations of High-frequency, Near-surface Internal Wave Groups in the Deep Ocean During GATE. Deep-Sea Research 1978, Vol. 25, pp. 299-307.

Tatarski, V.I., 1961: Wave Propagation in a Turbulent Medium, Chap. 4, McGraw-Hill, New York.

Thorpe, S.A. & Brubaker, J.M., 1983: Observations of Sound Reflection by Temperature Microstructure. Limnol. & Oceanogr. 28(4), 1983, pp. 601-613.

Thorpe, S.A., 1986: Bubble Clouds: A Review of Their Detection by Sonar, of Related Models, and of How K_v May be Determined. Oceanic Whitecaps (ed), pp. 57-68.

APPENDIX A

Calibration of Echosounder - CS-108

1. Source Level (SL):

The calibration of the 50 kHz echosounder was carried out in Woronora Dam. The arrangement of devices for calibration is shown in Fig.A1. The settings of the echosounder was:

G = 5
TVG = 10
Range = 60 m
Threshold = 0
Pulse Length = 1.632 ms (at max.)

The standard hydrophone used as a receiver for calibration had a receiving response at 50 kHz of -207 dB re 1 volt/μPa as stated in the manufacturer's calibration.

The depth and direction of the transducer was adjusted so that the hydrophone was at the centre of the the beam of the transducer.

The voltage of the received signal was:

$$V_{p-p} = 2 \text{ volt}$$

so

$$V_{eff} = \frac{V_{p-p}}{2\sqrt{2}} = 0.707 \text{ volt}$$

According to the definition of receiving response M:

$$M = 20\log\frac{V}{P}$$

where P is the acoustic pressure at the hydrophone, in μPascal.
V is output voltage of the hydrophone, induced by the acoustic pressure, in volt.

we have

$$\begin{aligned} 20\log P &= 20\log V - M \\ &= -3 + 207 \\ &= 204 \text{ dB re 1 } \mu\text{Pa} \end{aligned}$$

Since the source level is the acoustic pressure (P_1) measured one metre away from the emitting transducer over reference sound pressure, and

$$P_1 \cdot 1 = P \cdot r$$

where r is the distance between the transducer and the hydrophone, and was 3.048 m.

we have

$$\begin{aligned} 20\log P_1 &= 20\log P + 20\log r \\ &= 204 + 9.6 \\ &= 213.6 \text{ (dB) re 1 } \mu\text{Pa} \end{aligned}$$

so the source level is

$$SL = 20\log\frac{P_1}{P_0} = 213.6 \text{ dB re 1 } \mu\text{Pa}$$

where P_0 is the reference acoustic pressure. In here, it is 1 μPa.

2. The Relation Between Echo Level (EL) and the Colours Shown on the Screen of the Echosounder.

The calibration was also carried out in Woronora Dam. The arrangement of the devices for calibration is shown in Fig.A2. The settings of the 50 kHz echosounder is the same as that in Section 1 in Appendix A.

The standard hydrophone used as transmitter had a transmitting response at 50 kHz M = 137 dB re 1 μPa/volt.

Since the effective voltage of the transmitting signal V_1 = 28.28 volt, the transmitting sound pressure measured 1 m away from the hydrophone is

$$20\log P_1 = 20\log V_1 + M$$
$$= 166 \text{ dB re } 1 \mu\text{Pa}$$

The acoustic pressure received at the transducer is

$$20\log P_2 = 20\log P_1 - 20\log r$$

where r is the distance between the hydrophone and the transducer, is 4 m.

so $$20\log P_2 = 154 \text{ dB re } 1 \mu\text{Pa}$$

The voltage induced by this sound pressure P_2 at the transducer V_2 = 0.035 volt.

We can calculate the receiving response of the transducer

$$M' = 20\log V_2 - 20\log P_2$$
$$= -38.15 - 154$$
$$= -192.15 \text{ dB re 1 volt/}\mu\text{Pa}$$

The measurement of the internal circuit of the echosounder showed that a certain colour on the video display represents a certain 5dB range of the input voltage from the transducer (induced by the incident sound pressure). The relation between the colours and the input voltages is shown in Table A1.

Colour	Input Voltage (dB re 1volt)
red	-72
orange	-77
yellow	-82
dark green	-87
light green	-92
light blue	-97
mid-blue	-102

Table A1. Relation between colours and input voltage.

Consider the receiving response of the transducer M'and Table A1, we can find out the relation between colours and the echo level (acoustic pressure). See Table A2.

Colour	Echo Level (dB re 1μPa)
red	120.15
orange	115.15
yellow	110.15
dark green	105.15
light green	100.15
light blue	95.15
mid-blue	90.15

Table A2. Relation between colours and echo level.

3. Calibration for the Volume Backscattering Strength S

Eq.A1 is the formula for calculate the reverberation level (measured at the transducer) RL from volume scatterers

$$RL = SL + S + 10\log V - 40\log r - 2\alpha r \quad ...A1$$

where SL is the source level of the echosounder, in db.

S is the backscattering strength, in dB.

V is the scattering volume which equals to $V = \pi\theta^2 r^2 C\tau/2$ (see Fig.3.9).

where θ is half of beam width, in radius,

r is the range between the equivalent acoustic centre of volume scatterers and the transducer, in m,

C is the sound speed of the water, in m/s.

τ is the pulse length, in s.

α is the acoustic absorption coefficient, in dB/m.

$2\alpha r$ is very small in the near field and can be ignored. So we have

$$S = RL - SL - 10\log V + 40\log r \quad ...A2$$

For the echosounder used, we know

$$SL = 213.6 \text{ dB}$$

$$\theta = 9^{\circ}\pi/180^{\circ}$$

$$\tau = 0.001632 \text{ s}$$

and we assume the speed of sound C = 1450 m/s.

By substituting all these into Eq.A2, we get

$$S = RL + 20\log r - 203.2 \text{ dB} \qquad \ldots A3$$

Now using Eq.A2 and referring to Table A2, we can easily calculate the backscattering strength S when the "colour" of the reverberation level RL is known and the range r is given. The result is shown in Fig.A3.

4. Calculation of Reflection Coefficient of Sheet Reflectors

When a sound wave is normally incident onto a layer of sheet reflectors (see Fig.A4), only the reflections from those sheet reflectors whose thickness is half of the transmitting pulse length can be received at the same time (see Pg.29).

If we assume that the reflection coefficient of each sheet is very small and that multiple reflections can be ignored (see Appendix B), we can calculate the echo level from the sheet reflectors as

$$EL = SL + 10\log R - 20\log(2r) \qquad \ldots A4$$

where SL is the source level of the echosounder,
R is the reflection coefficient of the layer of sheet reflectors.
r is the range from the transducer to the sheet reflector.

Since SL = 213.6 dB, we can change Eq.A4 into

$$10\log R = EL + 20\log r - 207.6 \qquad \ldots A5$$

We can also get the reflection coefficient when the "colour" of the echo and the range are given. (See Fig.A5)

APPENDIX B

Procedure of Proving "Multiple Reflections Can be Ignored" and "$R = \sum_{j=1}^{n} R_j \exp(-i2kjd)$"

1. Multiple Reflections Can Be Ignored

Consider a free plane sound wave, normal incident at a fluid layer with a constant sound speed gradient G (See Fig.3.2). D is the thickness of the layer. The linear layer is divided into n thin layers with equal thickness δz which is so small that each thin layer can be treated as a constant sound speed layer.

Fig.B1 shows the first acoustic reflections and second back-reflections from a layered medium. We give definitions to the first and second back-reflection as

(1) Back-reflection - the sound reflection ray towards the sound source.
(2) First reflection - the sound ray induced by the incident sound that is reflected by the interface of the layers only once.
(3). Second back-reflection - the sound ray induced by the incident sound that is reflected by the interfaces three times, travelling in the opposite direction (to the incident sound).
(4). Multiple reflections - the sound reflection rays that have been reflected by the interfaces of the layers more than once.

Firstly, we prove that the second back-reflections are much weaker than the first ones that they can be ignored.

We adopt the 4 simplifications in Section 3.2 in Chapter 3, and make one assumption: all first and second back reflections from n interfaces of n thin layer have the same phase at the observing point z = 0. (This is based on the prerequisition: $D \ll \lambda$. See the first requirement for numerical technique in Section 3.3 in Chapter 3.)

Normally, the reflection coefficient from sound speed structure is very small. It can be less than 10^{-4} if δz is small enough.

So that the refraction coefficient w equals 1 is a reasonable approximation. Then we can assume that the incident sound pressure remains constant when the sound wave is propagating through the layers.

If the incident sound pressure is p_i and the reflection coefficient of each thin layer (sound speed step) is δR, then the sound pressure of the first back reflections all n thin layers is

$$p_i n \delta R = p_i n \frac{G \delta z}{2C_0} = p_i \frac{GD}{2C_0}$$

(See also Eq.3.22 in Chapter 3)

The number of second back-reflections is (see Fig.B1)

$$N = 1^2 + 2^2 + 3^2 + 4^2 + \cdots + (n-1)^2$$

$$= 1/6(n-1)n(2n-1)$$

Because n is a big number, we have

$$N \approx n^3/3$$

Then the sound pressure of all second back reflections is

$$p_i N(\delta R)^3$$

The ratio of the sound pressure of the second back reflections to the first ones becomes

$$\frac{p_i N(\delta R)^3}{p_i n \delta R} = \frac{n^2}{3}(\delta R)^2$$

$$= \frac{1}{3}\left(\frac{GD}{2C_0}\right)^2$$

because

$$\left|\frac{GD}{2C_0}\right| = \left|\frac{C_0 - C_D}{2C_0}\right| << 1$$

so

$$\frac{p_i N(\delta R)^3}{p_i n \delta R} << 1$$

This means the second back-reflections are very weak compared with the first ones and can be ignored.

On the same principles, we can prove that the third and higher order back-reflections are much weaker than the second ones. So the multiple reflections can be ignored.

2. $R = \Sigma R_j \exp(-i2kjd)$

To prove this, we consider a normal incident sound wave on a sound velocity structure which is divided into n thin constant sound speed layers, or steps (see Fig.3.2). The incident sound pressure can be expressed as

$$P = P_i \exp(-ikz)$$

and the reflection is a composite wave which is the sum of all reflections from n thin layers, including the first reflections and multiple reflections. Since we have ignored multiple reflections, the composite wave is the sum of n first-reflections from n thin layers. This is

$$P_r = \sum_{j=1}^{n} P_j \exp(-i2kz)$$

where P_j is the amplitute of the sound pressure reflected from Number j step.
k is the wave number.
z is the depth of Number j step. If the numerical step size is d, then $z = jd$.

And the reflection coefficient from Number j step R_j is identical with the one when other steps are absent, which is illustrated in Eq.3.20. Thus the amplitute of sound pressure reflected by Number j step is

$$P_j = R_j P_i$$

and the total reflection from all n steps is

$$P_r = \sum_{j=1}^{n} P_j \exp(-i2kz)$$

$$= \sum_{j=1}^{n} R_j P_i \exp(-i2kjd)$$

Finally we can get the complex reflection coefficient of n thin layers

$$R = \frac{P_r}{P_i} = \sum_{j=1}^{n} R_j \exp(-i2kjd)$$

APPENDIX C

On The Two Requirements of The Numerical Technique

1. Numerical Step Size Must Be Equal To Or Smaller Than $\lambda_o/4$

The analysis is based on Eq.3.33 which is for calculating the reflection coefficient of sound velocity microstructure:

$$R = \frac{1}{4\pi F} \sum_{j=1}^{n} G_j \sin(k_0 d)[\cos k_0(2j-2)d - i \sin k_0(2j-1)d]$$

The phase consists of two parts:

the real part: $\cos k_0(2j-1)d$

and the imaginary part: $\sin k_0(2j-1)d$

We can only discuss one of them because there are the same except a phase difference of $\pm\pi/2$.

Fig.C1 shows the variation of $\sin k_0(2j-1)d$ versus j, where j is the ordinal number of thin layers divided. The phase difference between the reflections from the adjacent layers, e.g. Number j layer and Number j+1 layer, is

$$k_0[2(j+1)-1] - k_0(2j-1)$$
$$= 2k_0 d$$

At least two samples per cycle are required to define a sine (or

cosine) component (see p229, Bendat & Piersol, 1971). i.e.

$$2k_0 d \leq \pi$$

or $$d \leq \lambda_o/4$$

This requirement is technically sufficient for sampling the phase of the numerical steps.

2. Numerical Step Size Must Be Much Smaller Than The Thickness of The Fluctuation With The Smallest Vertical Scale in The Sound Velocity Microstructure

The numerical technique is a model approaching a true sound velocity microstructure with a large number of linear layers. If the size of the linear layer is sufficiently small, the approaching will fail.

The sampling of a temperature microstructure with PORPUS is performed at equal vertical intervals (Fig.3.8). The poblem then is to determine an appropriate sampling separation, d. We assume there is a fluctuation with the smallest vertical scale, h, as shown in (a), Fig.C2. When the sampling separation becomes bigger and bigger, the linear layer approaching model will go apart from the true temperature profile, as illustrated in (b), (c) and (d) in Fig.C2. This will lead to an increasing error when applying Eq.3.33 for calculating the acoustic reflection coefficient from temperature microstructure. Thus

$$d \ll h$$

is a requirement for the numerical technique.

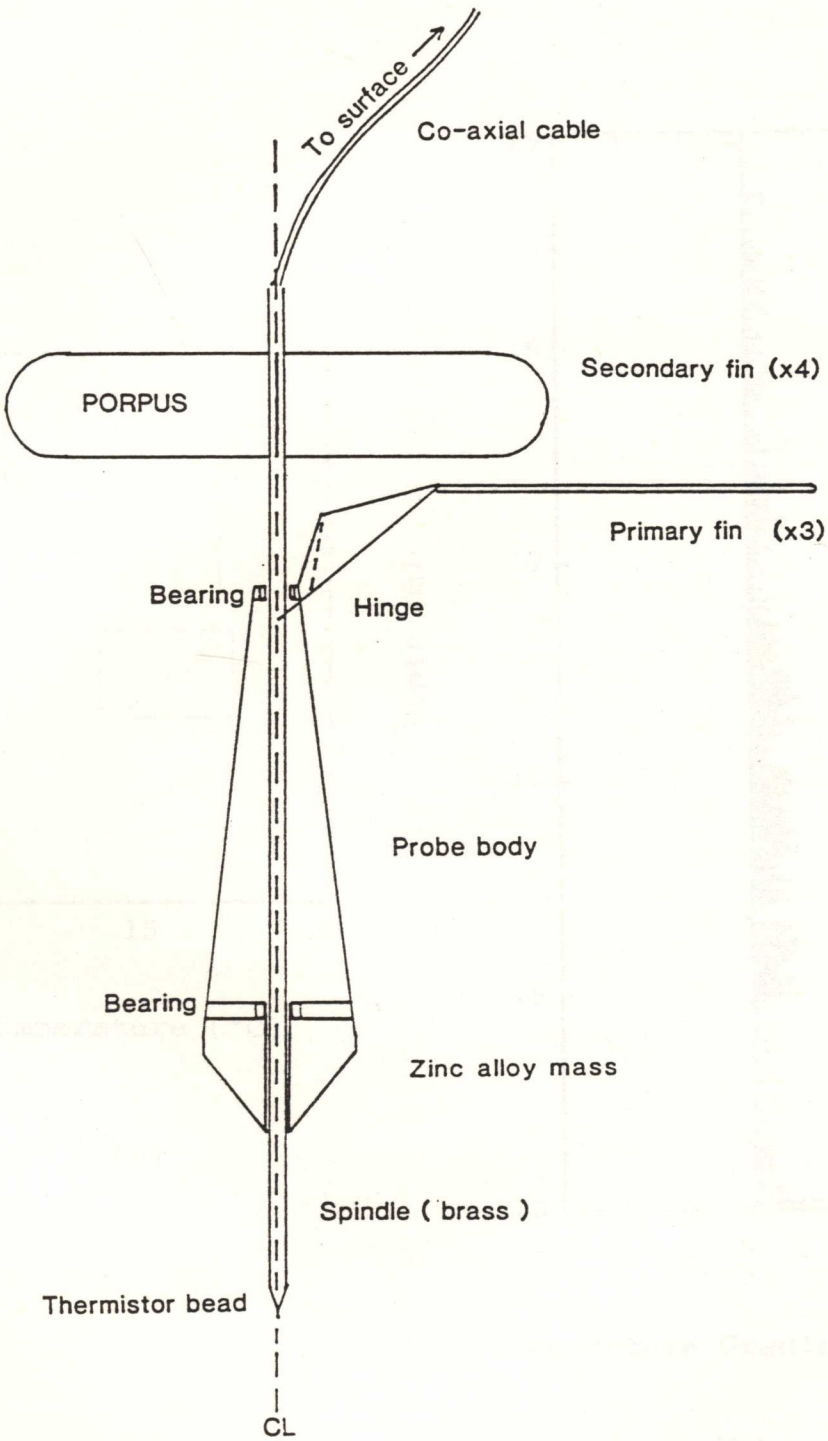

Fig.2.1 Schematic of PORPUS.

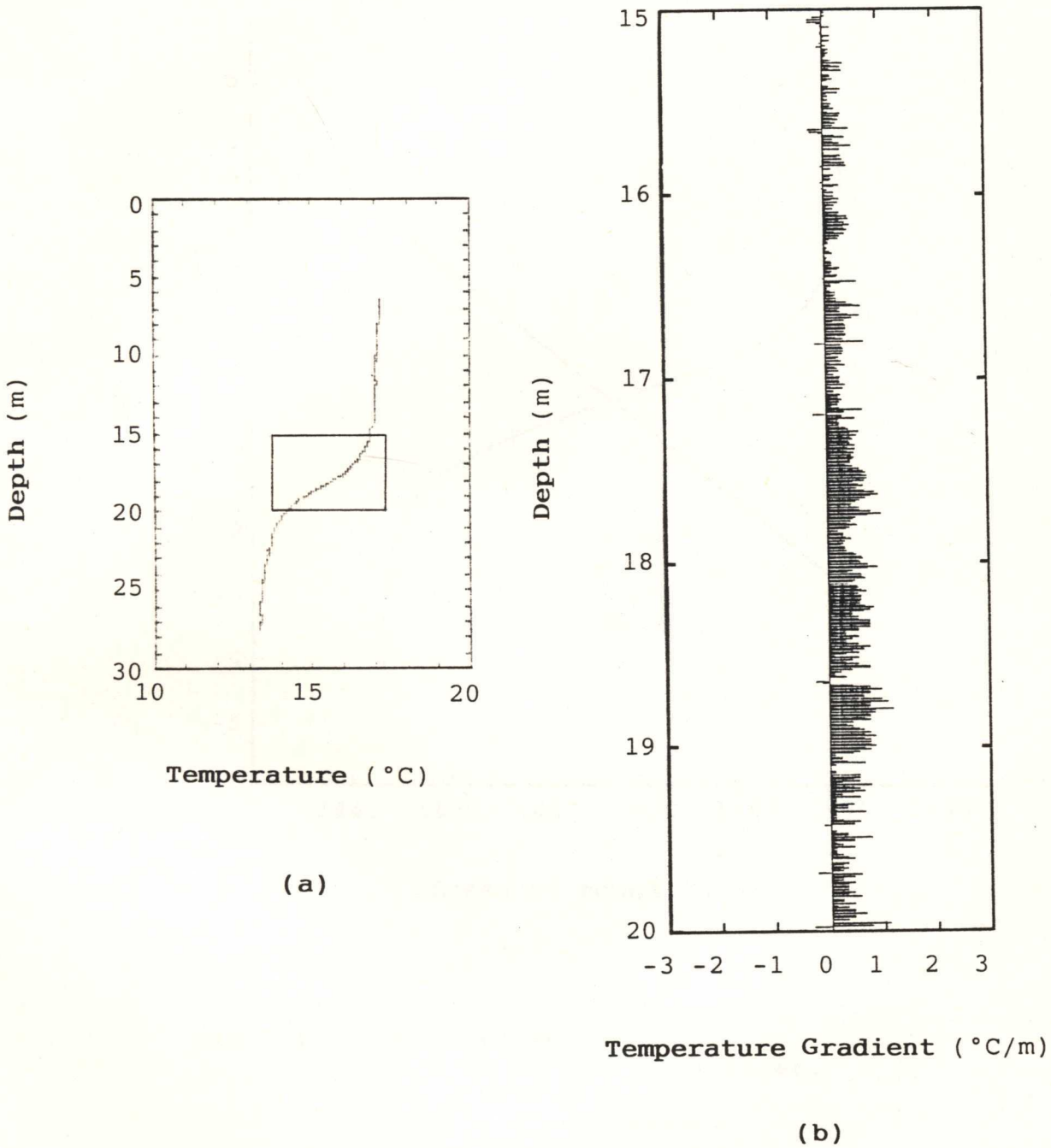

Fig.2.2 Temperature microstructure measured with PORPUS in Woronora on 25/5/89.
(a) is the temperature profile.
(b) is the temperature gradient within the "box" shown in (a).

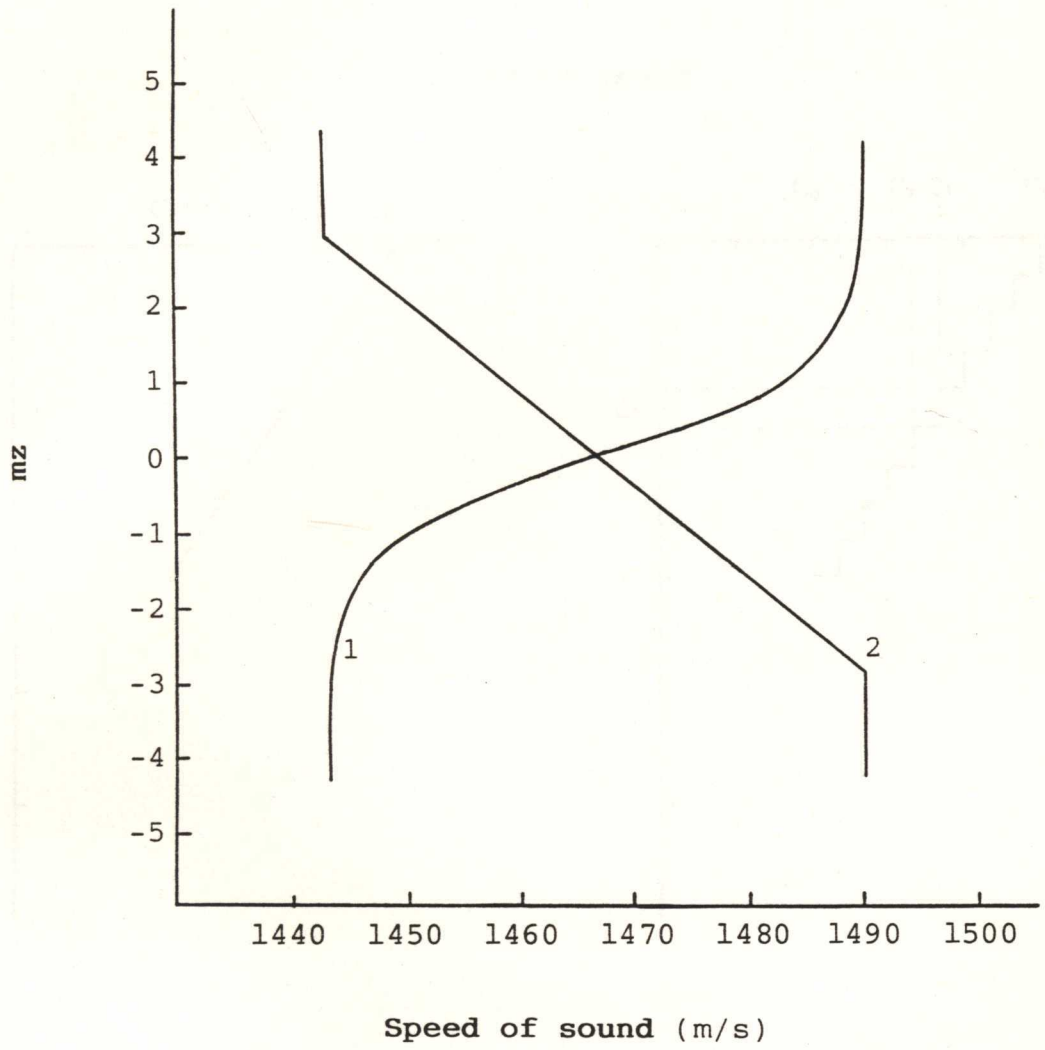

Fig.3.1 Two transition layers.
Curve 1, a transitional layer.
(N=0.06)
Curve 2, a linear layer.
(A=-32)

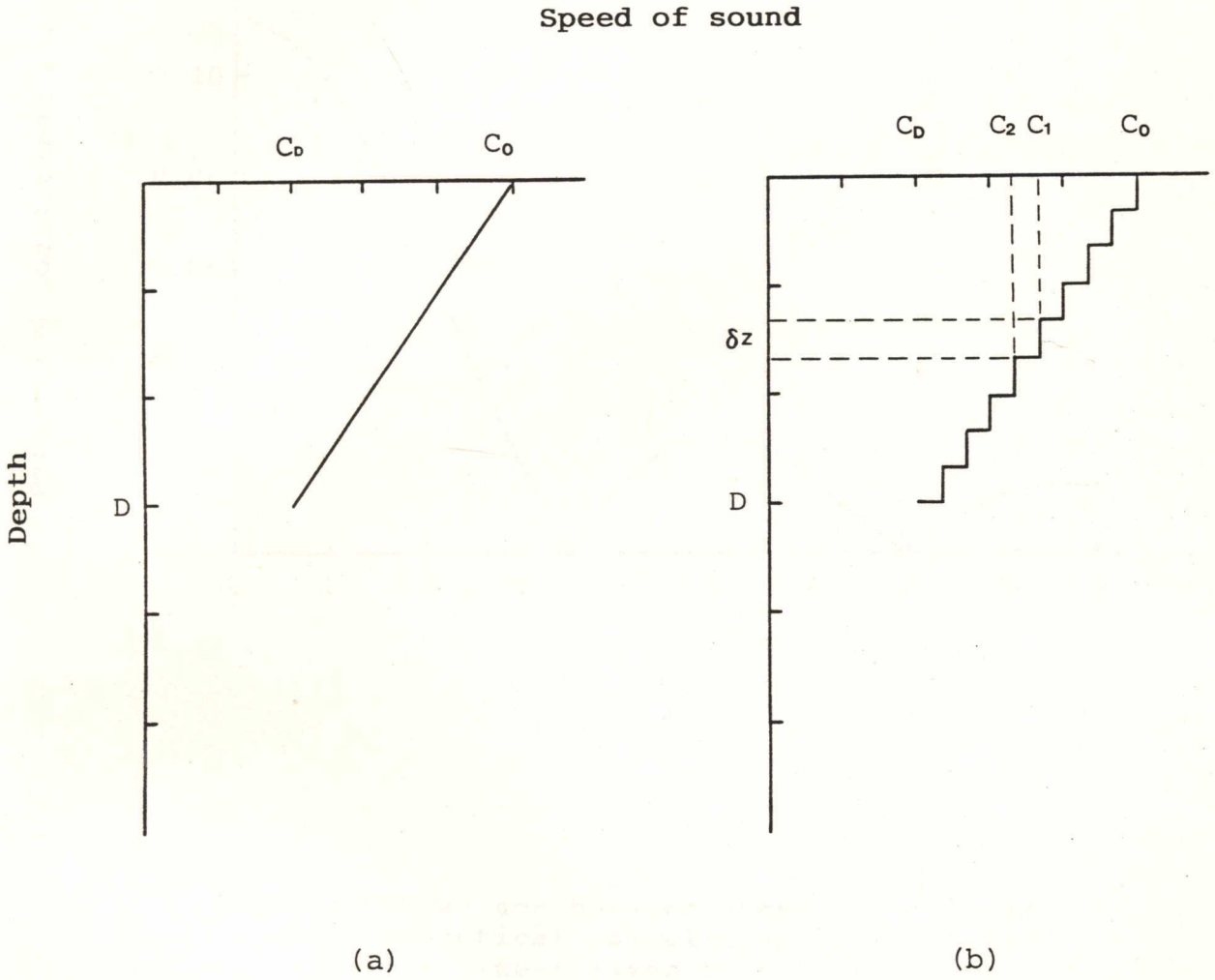

Fig.3.2 Sound velocity structure.
A linear layer (a) is replaced
by a number of steps (b).

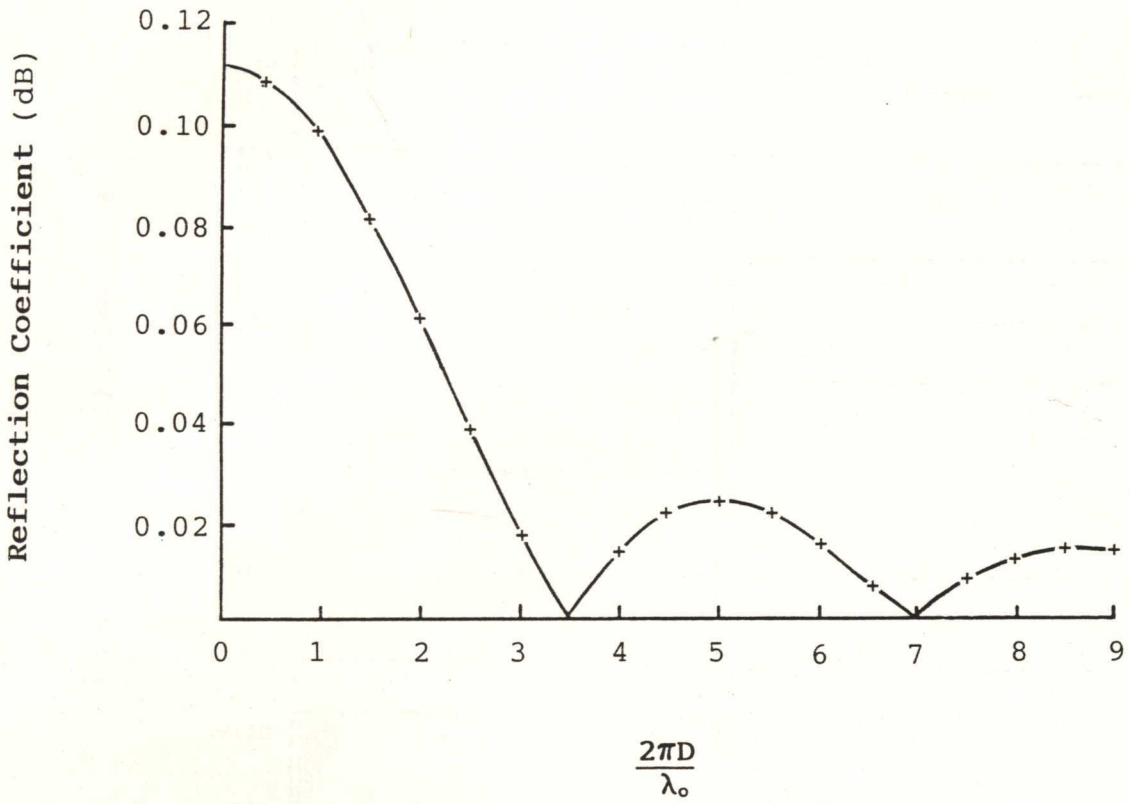

Fig.3.3 Comparison between numerical (+) and theoretical calculation (solid line) of a linear layer as a function of the thickness of the layer.

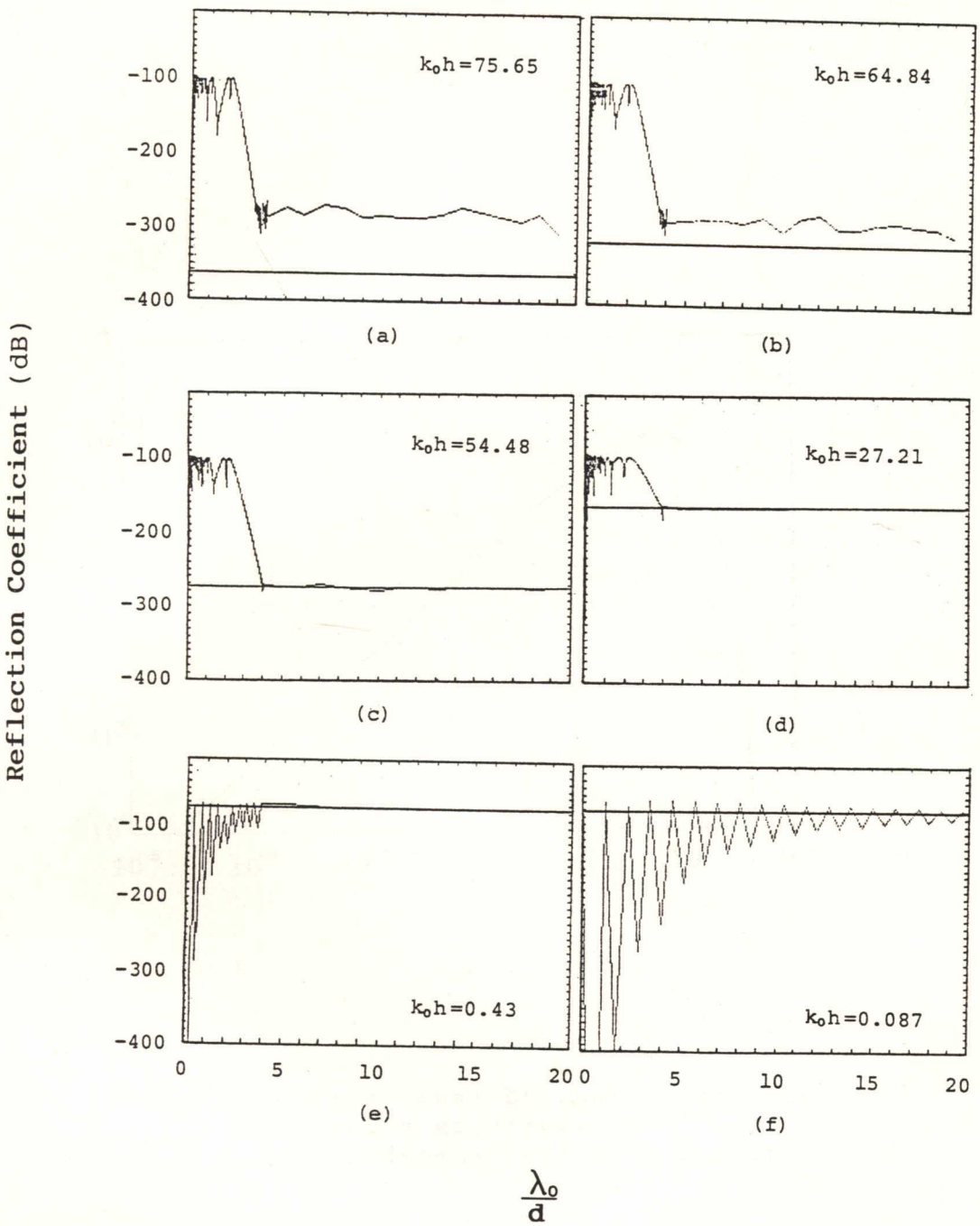

Fig.3.4 Numerically calculated, 50 kHz reflection coefficient of the transitional layers with different thickness.

The horizontal straight lines are the theoretical results, which increase when $k_0 h$ decreases, where h is the thickness of the layer.

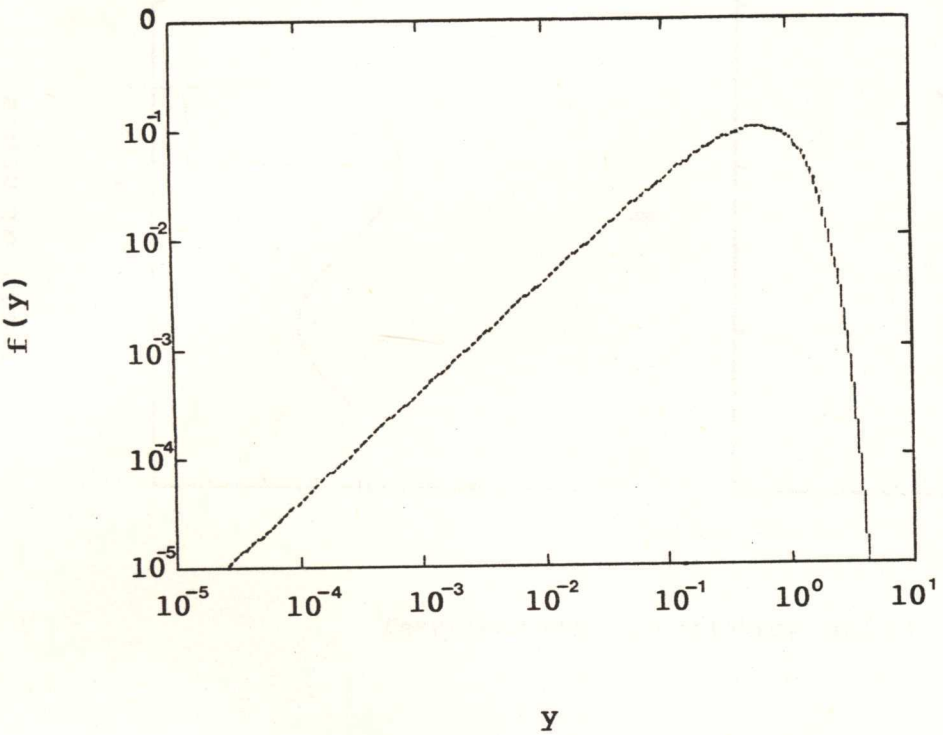

Fig.3.5 One-dimensional Batchelor spectrum for temperature gradient.
y is non-dimensional wave number.

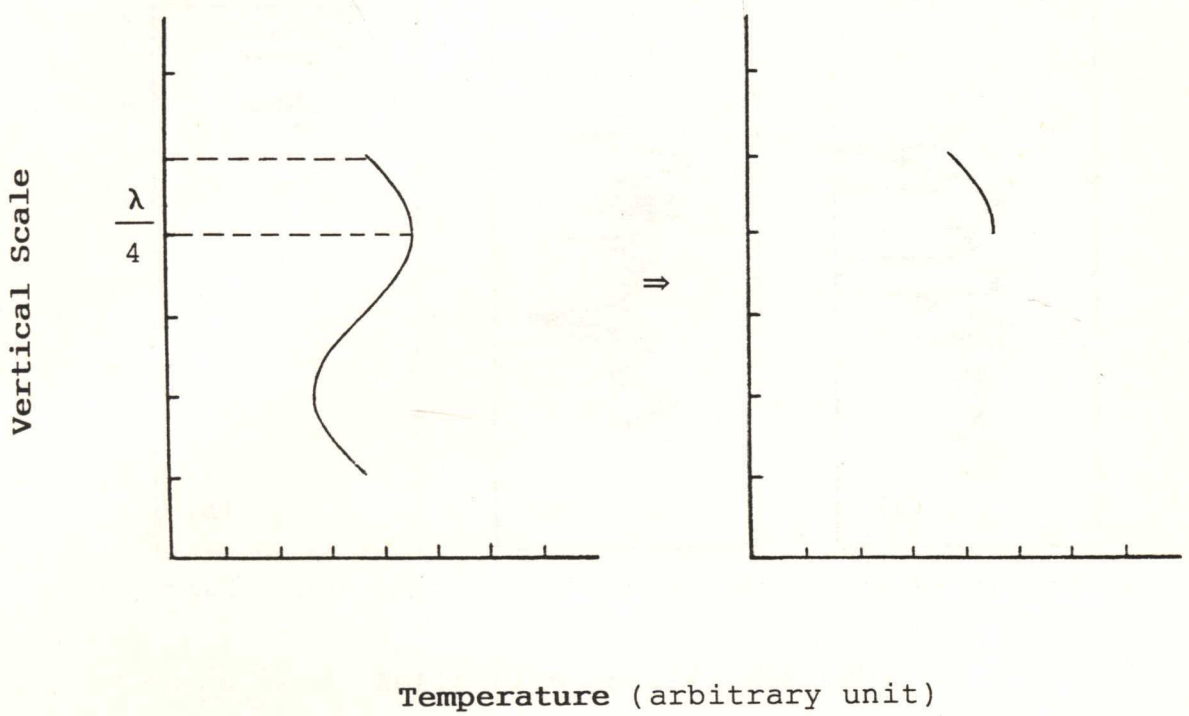

Fig.3.6 λ/4 temperature step.

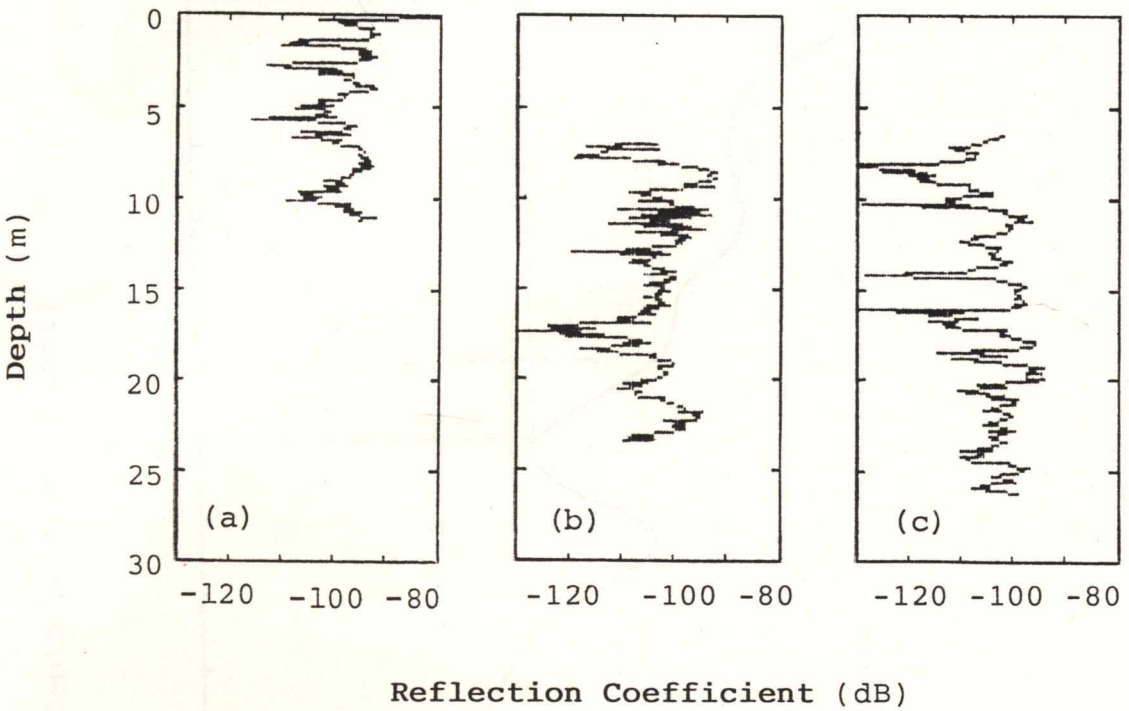

Fig.3.7 The 50 kHz reflection coefficient profiles of temperature microstructure measured in Woronora Dam on 8/8/88 (a), 6/12/88 (b) and 25/5/89 (c).

The following conditions apply:
$d = 0.7097$ cm
$\lambda_o = 2.96$ cm
where d is the sampling separation,
λ_o is the acoustic wave length.

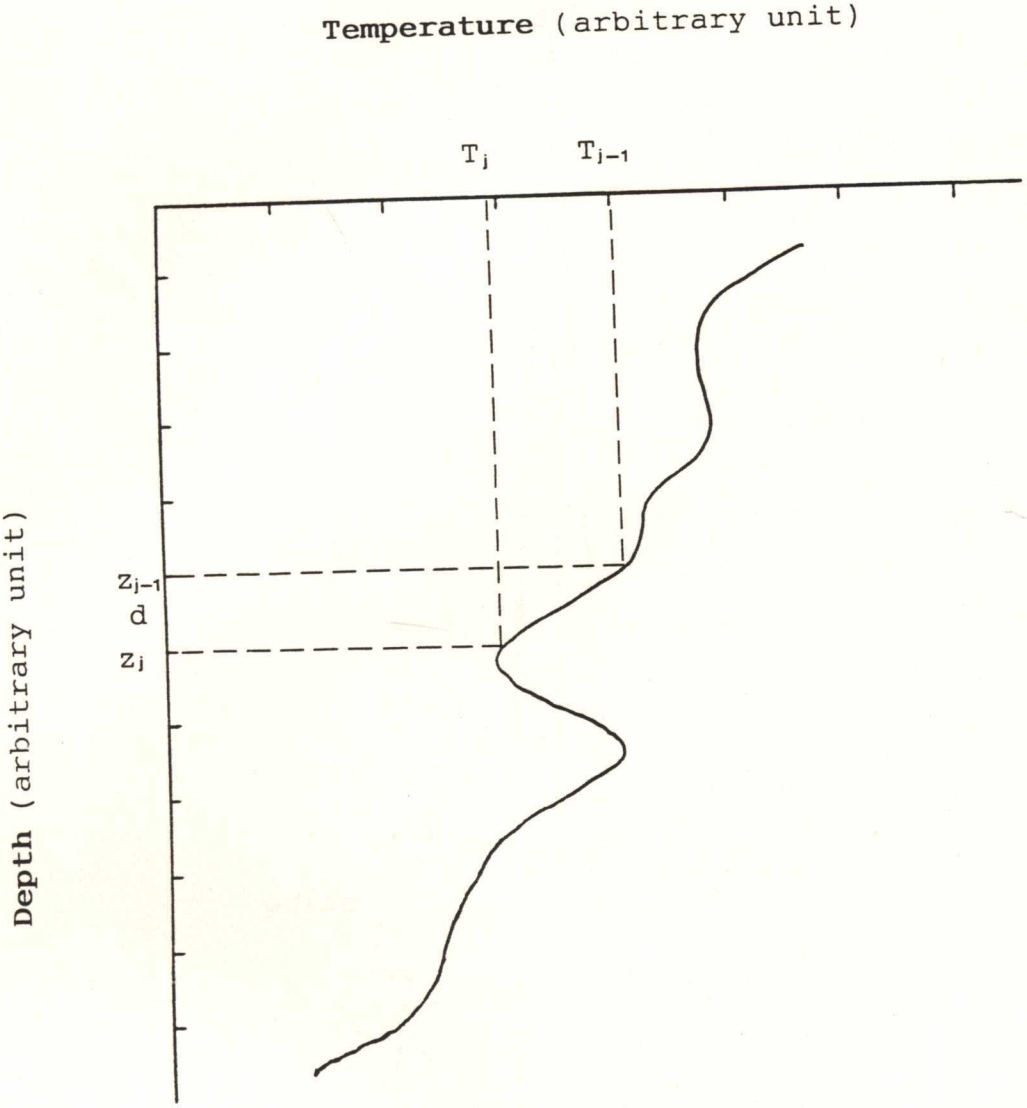

Fig.3.8 Details of temperature microstructure.

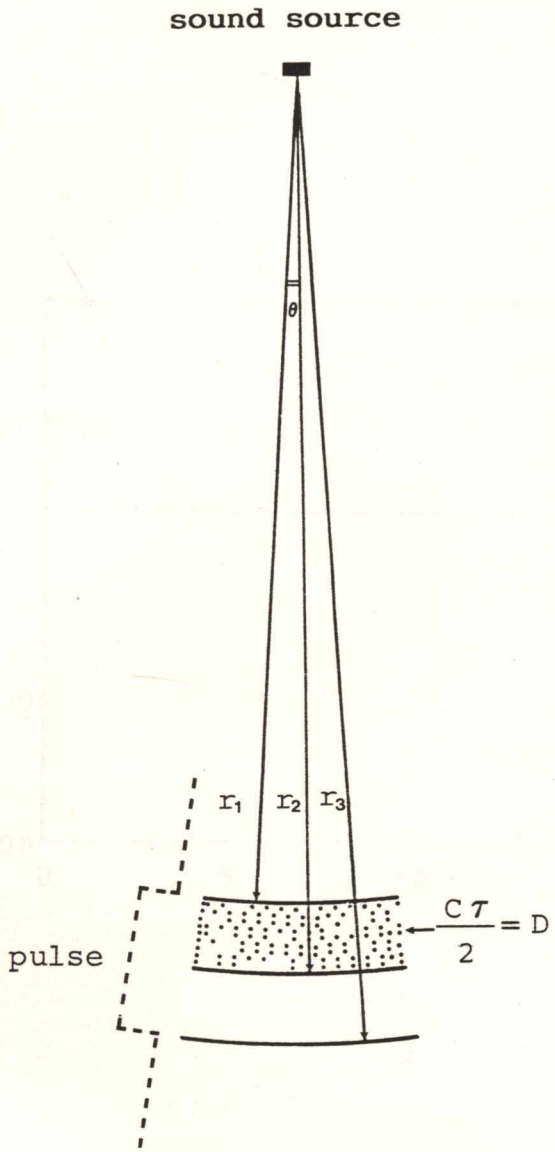

Fig.3.9 Cτ/2 reflection layer.
C is speed of sound.
τ is the pulse duration.

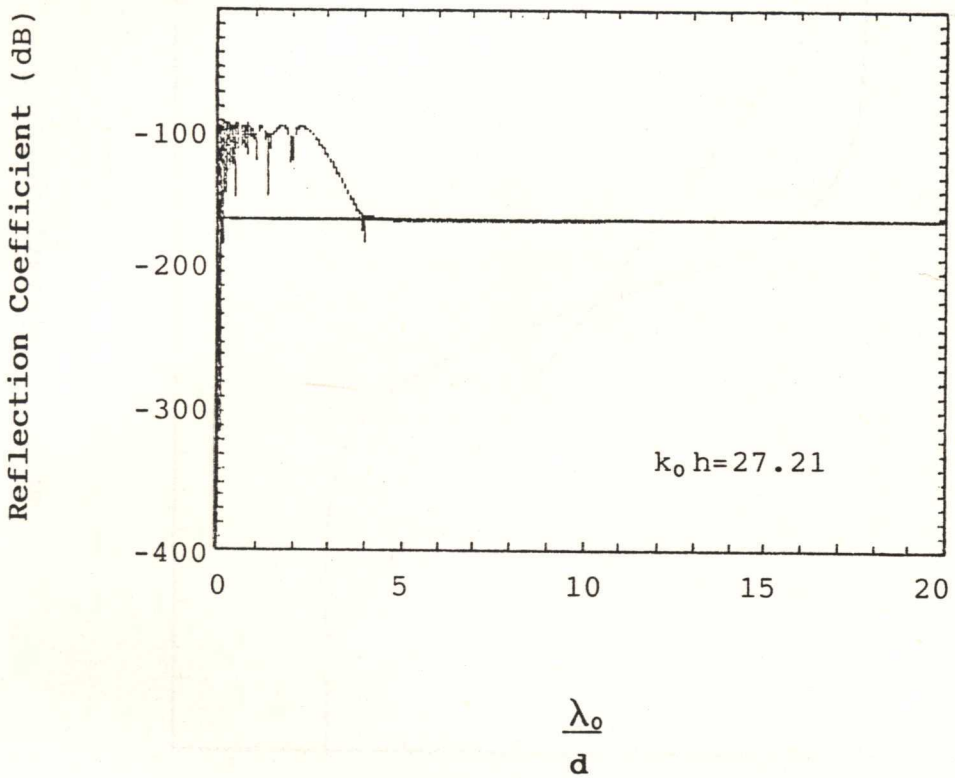

Fig 3.10 Error occuring when
$\lambda_o/d < 4$.
where λ_o is the acoustic wave length.
d is the numerical step size.

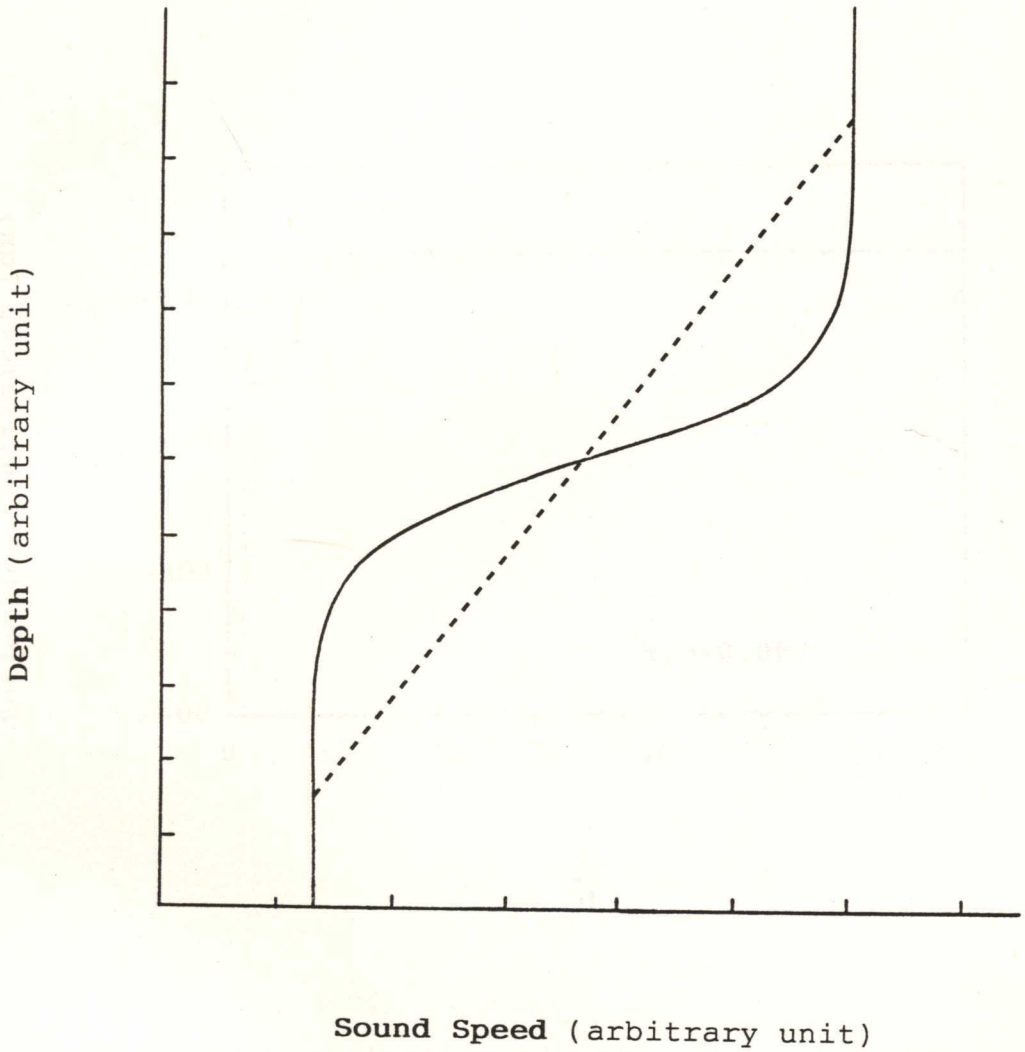

Fig.3.11 The transitional layer is replaced by a linear layer whose thickness is larger.

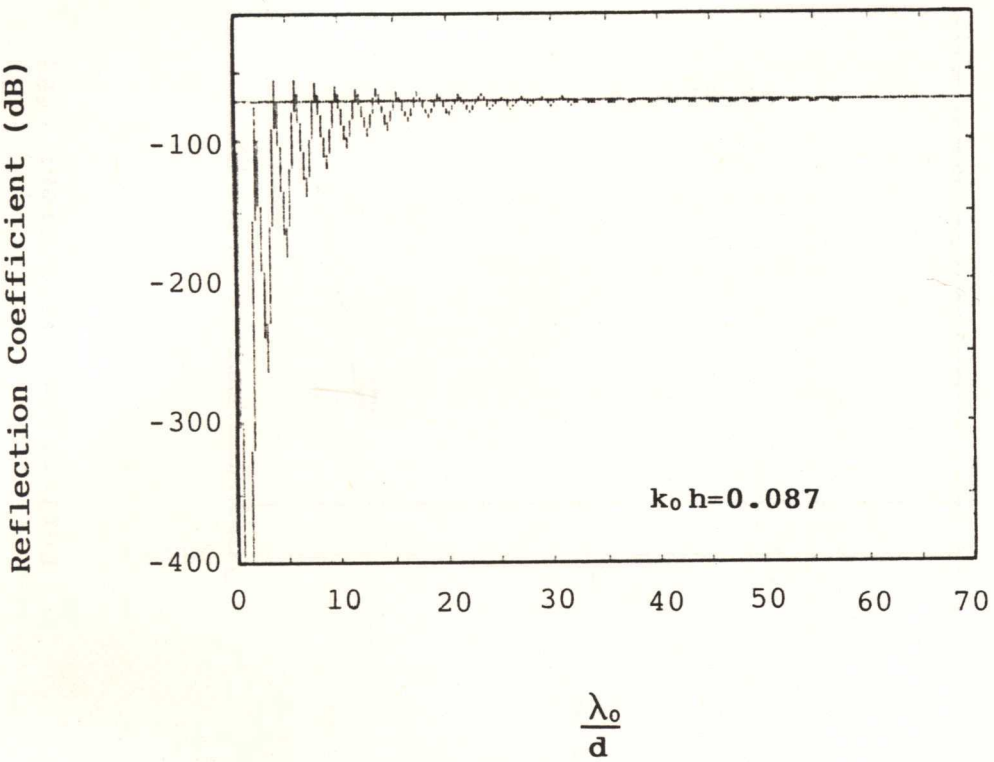

Fig 3.12 Numerical result when the thickness of the transitional layer is smaller than the numerical step size:
$d \gg h$.
Horizontal line is the theoretical result.

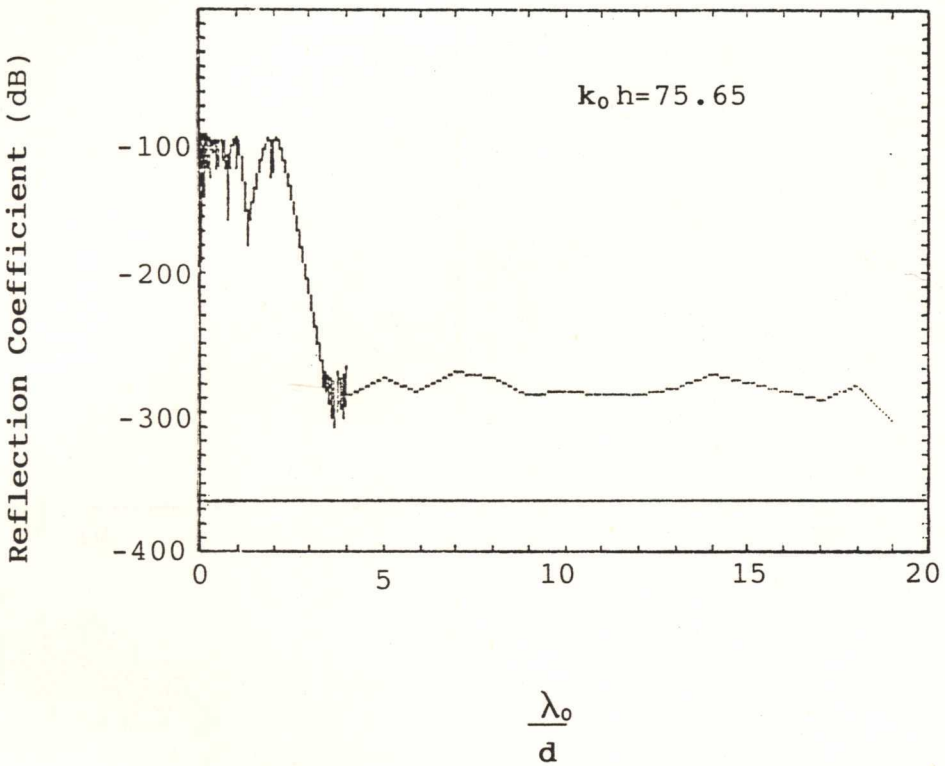

Fig.3.13 The numerical result can't match the theoretical one when it is beyond the limit of computer precision. (N=0.001, m=0.36)

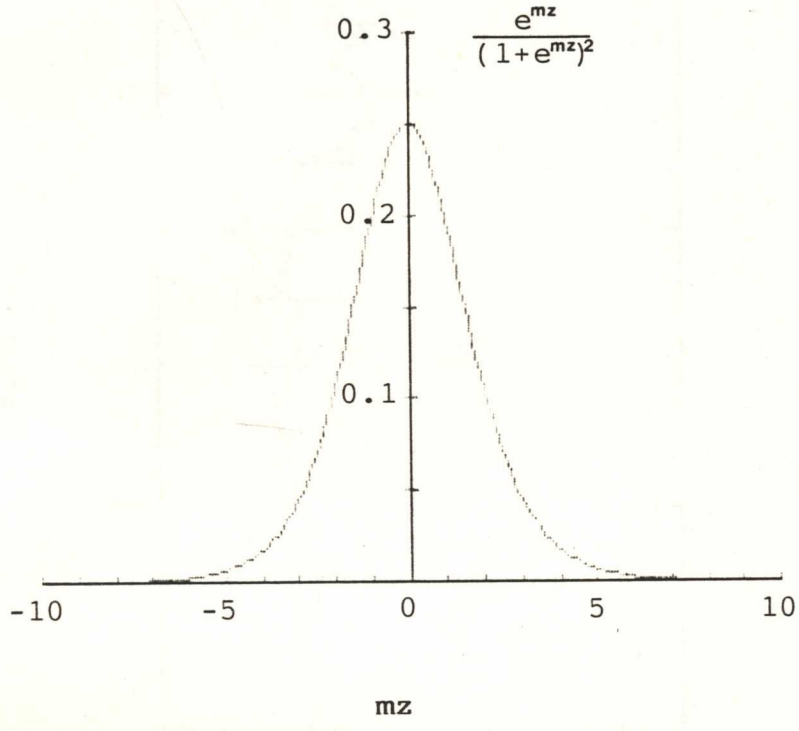

Fig.3.14 $\frac{e^{mz}}{(1+e^{mz})^2}$ versus mz.

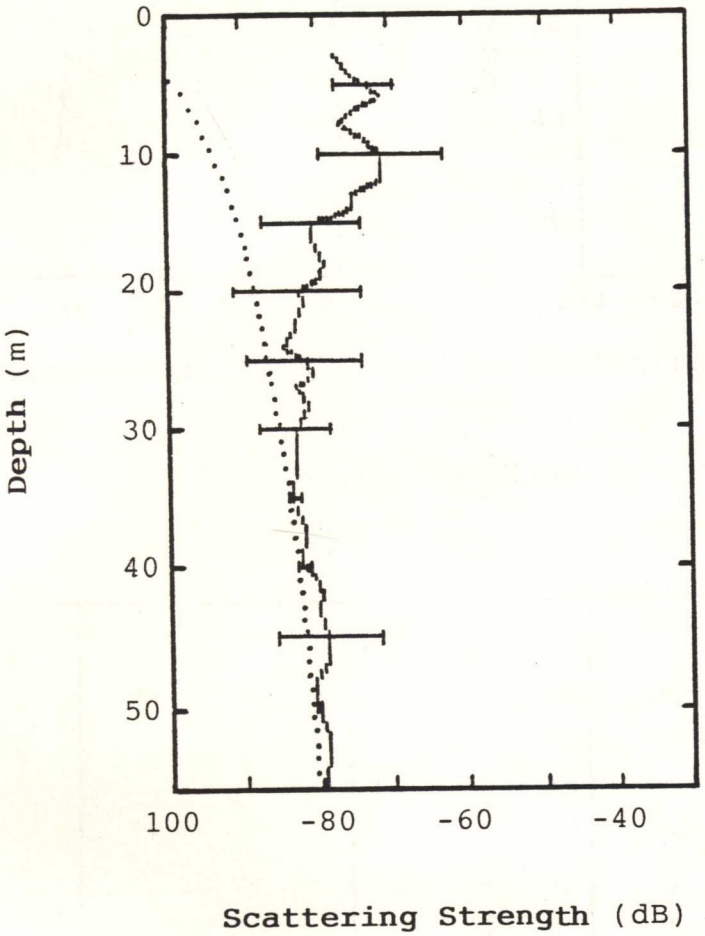

Fig.4.1 Averaged acoustic backscatter profile at 50 kHz in Woronora.
Dotted line shows the threshold of the echosounder.

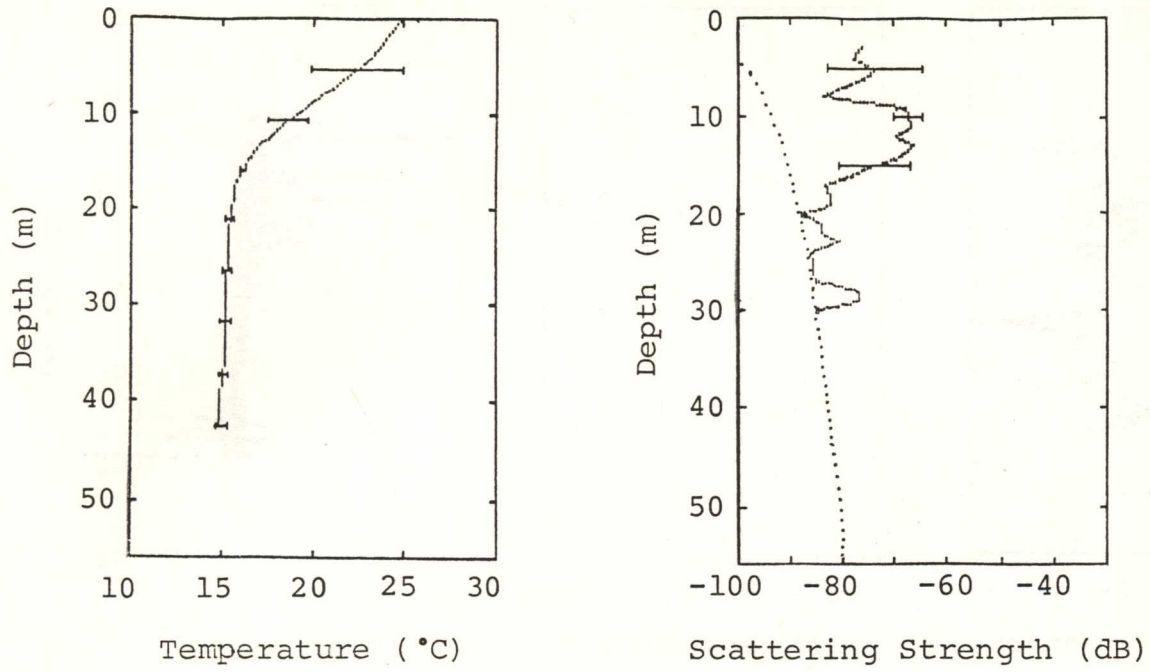

Summer Profiles

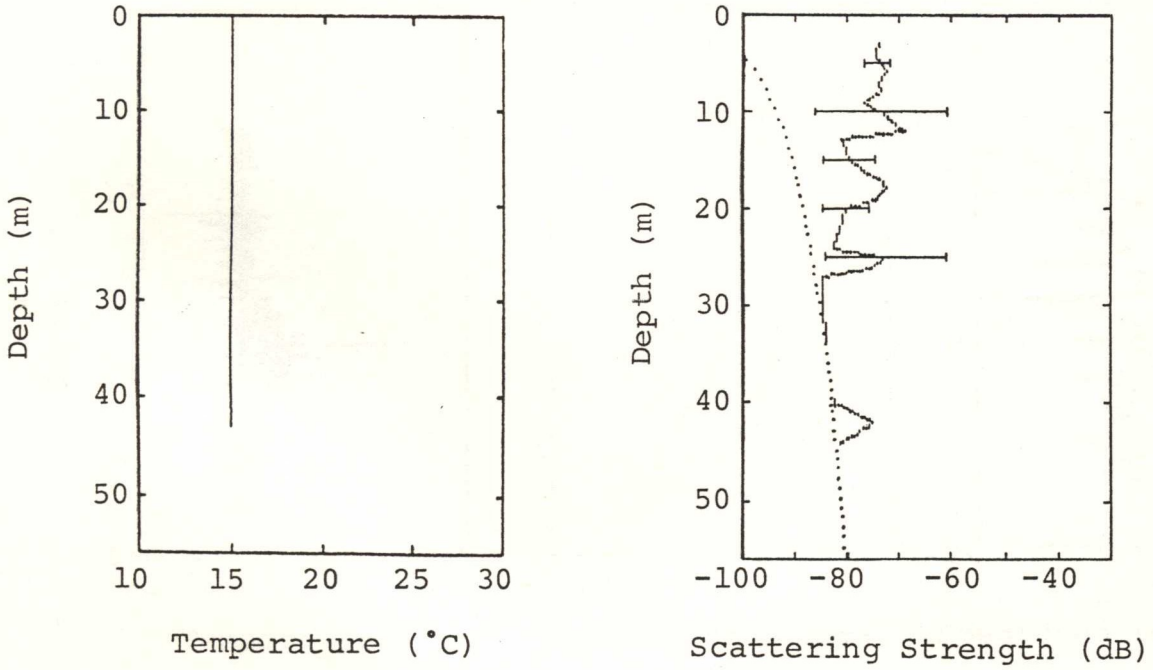

Winter Profiles

Fig.4.2 Comparison between temperature gradient and 50 kHz acoustic scattering strength. Dotted line shows the threshold of the echosounder.

This figure demonstrates that the measured acoustic scattering does not appear to be correlated with the temperature gradient.

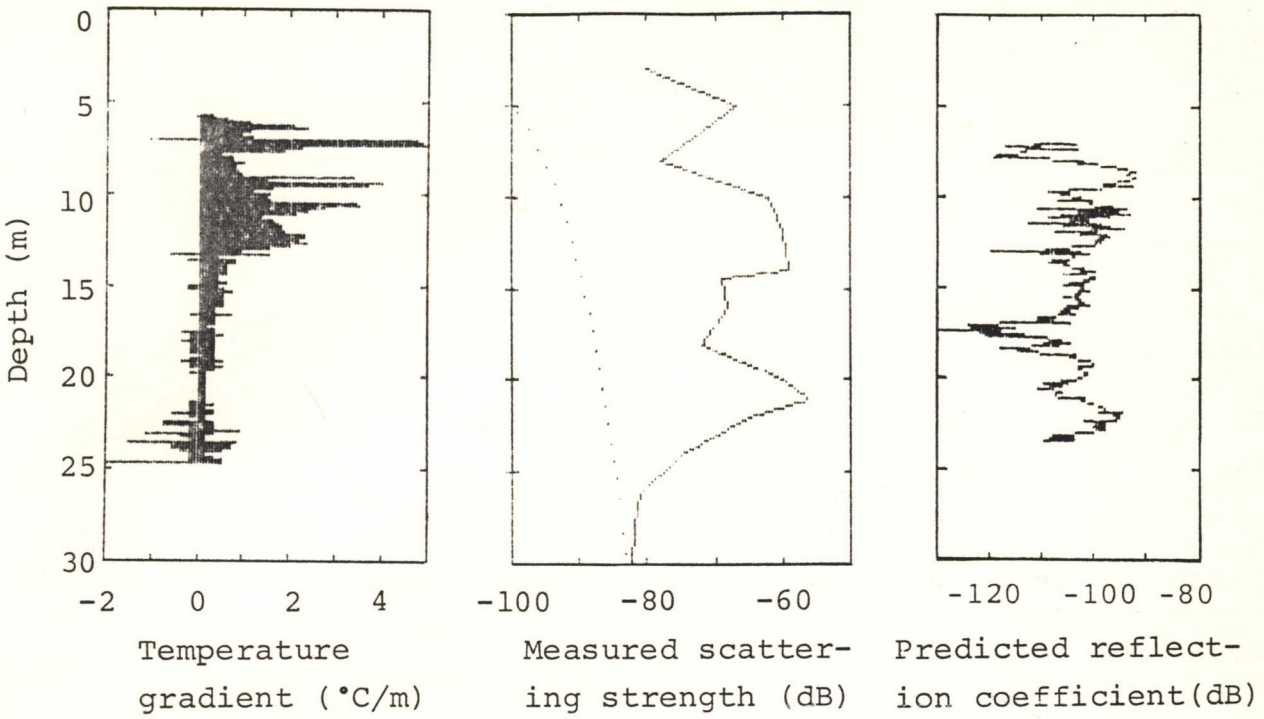

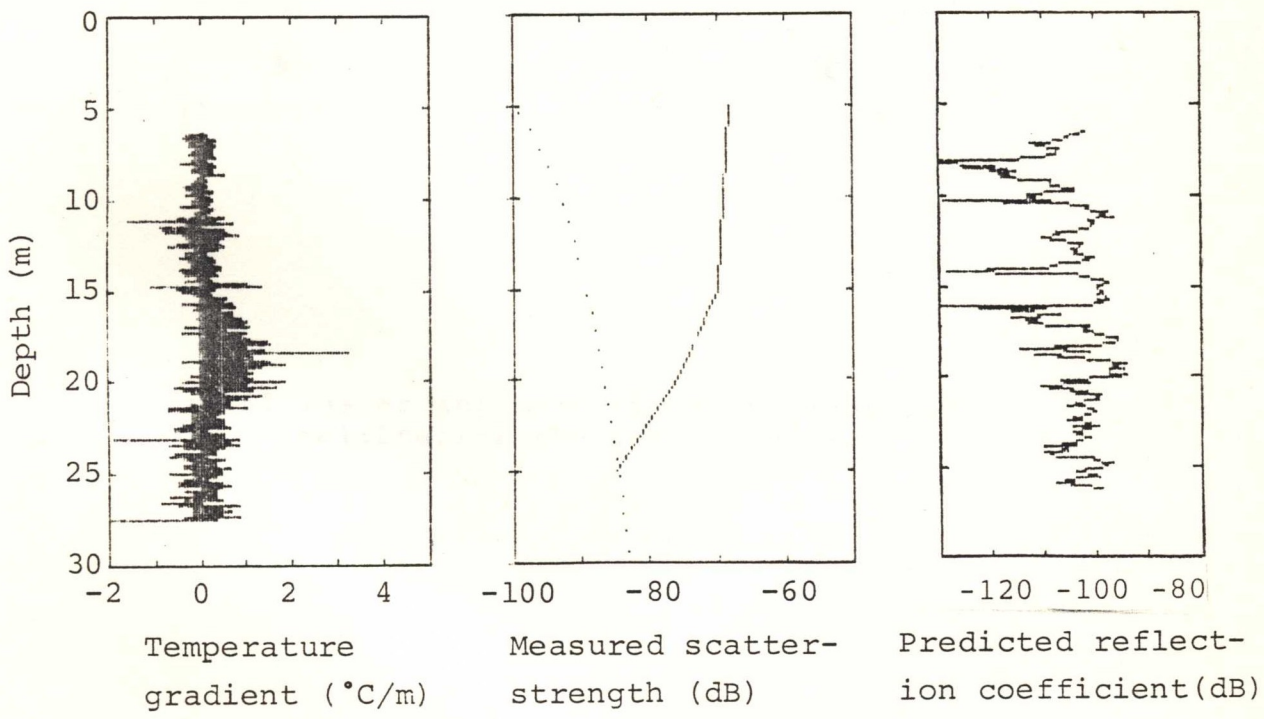

Fig.4.3 Comparison of simultaneously measured temperature microstructure, observed acoustic scattering and predicted acoustic reflection from microstructure. The predicted due to microstructure is much less than the observed while the observed appears to be independent of the microstructure level. Dotted line is the threshold of the echosounder.

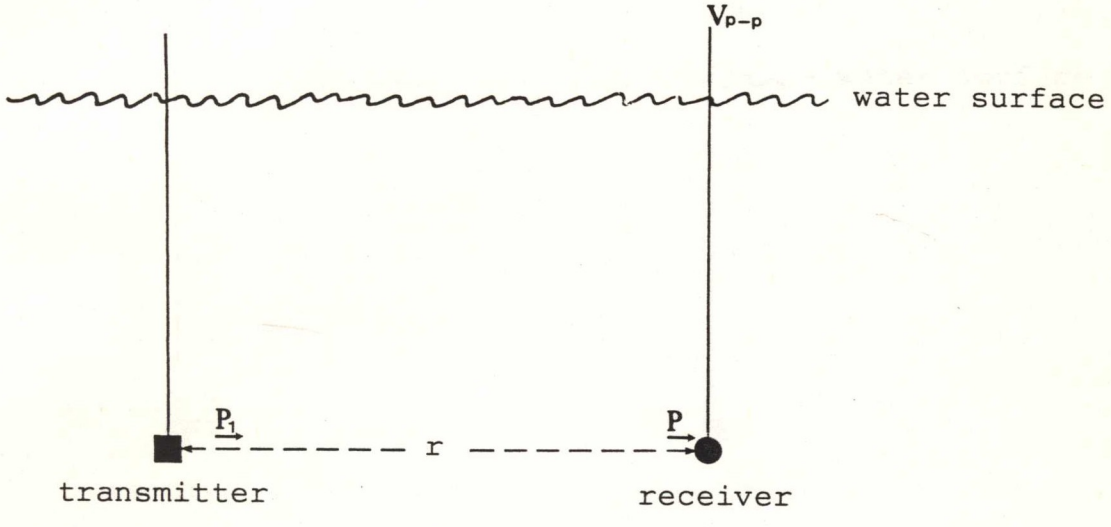

Fig.A1 The arrangement of the devices for calibrating the source level.

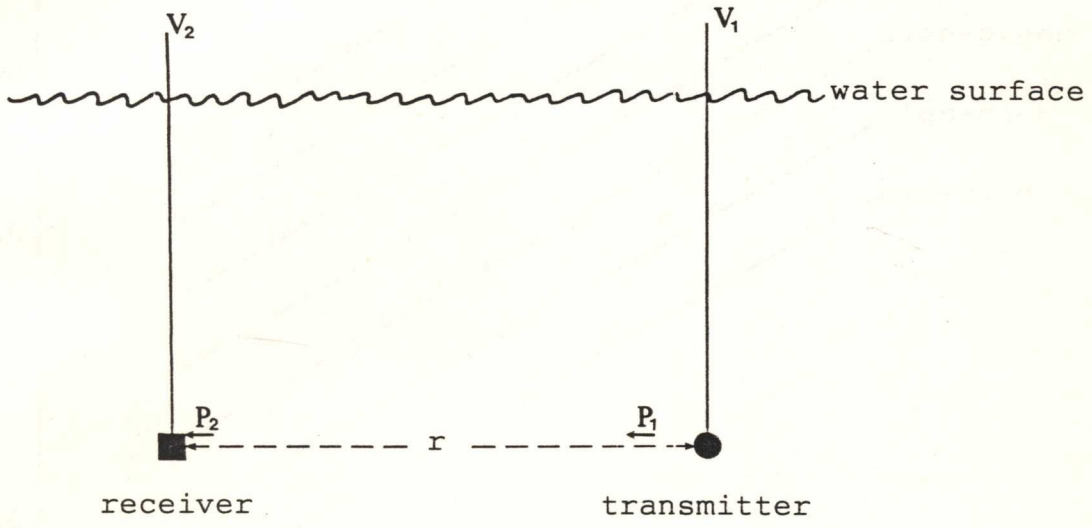

Fig.A2 The arrangement of the devices for calibrating the receiving response.

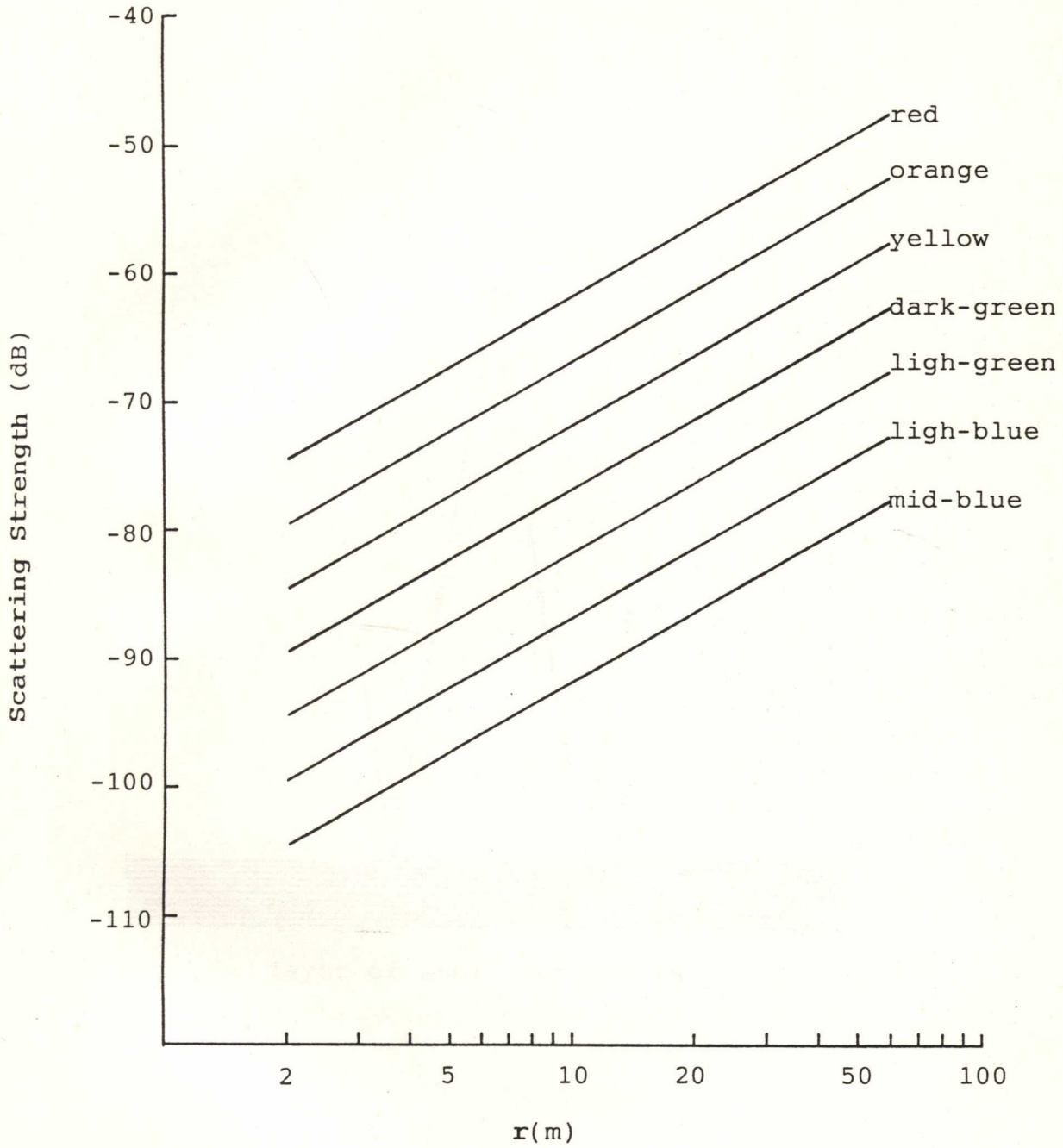

Fig.A3 The relation between backscattering strength and the colours shown on screen as a function of range.

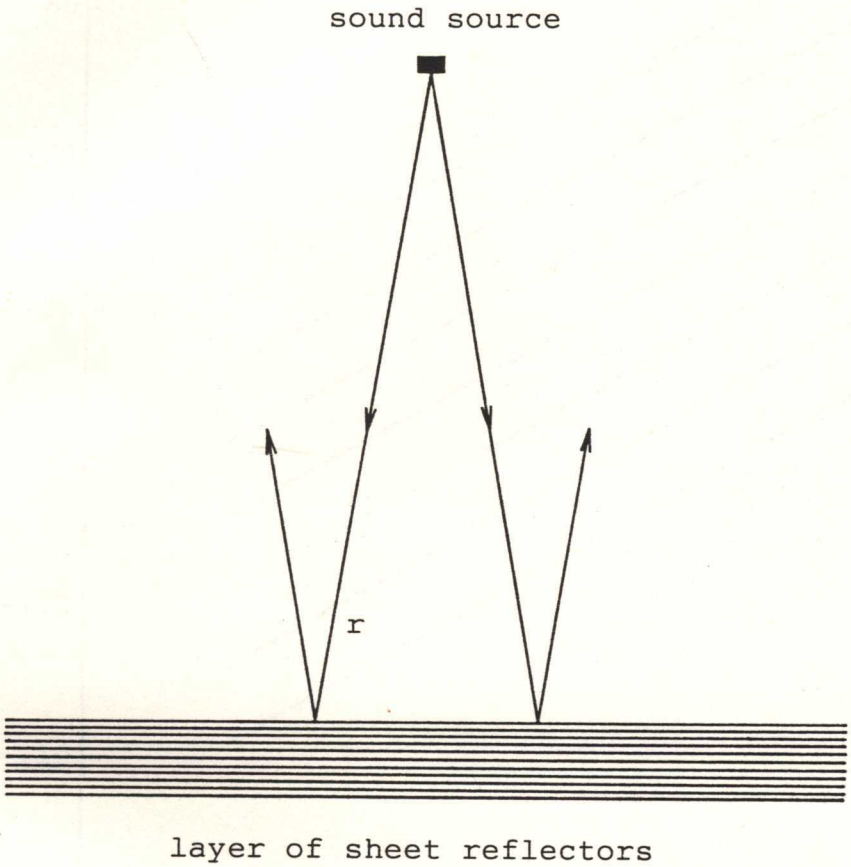

Fig.A4 Reflection from a layer of sheet reflectors.

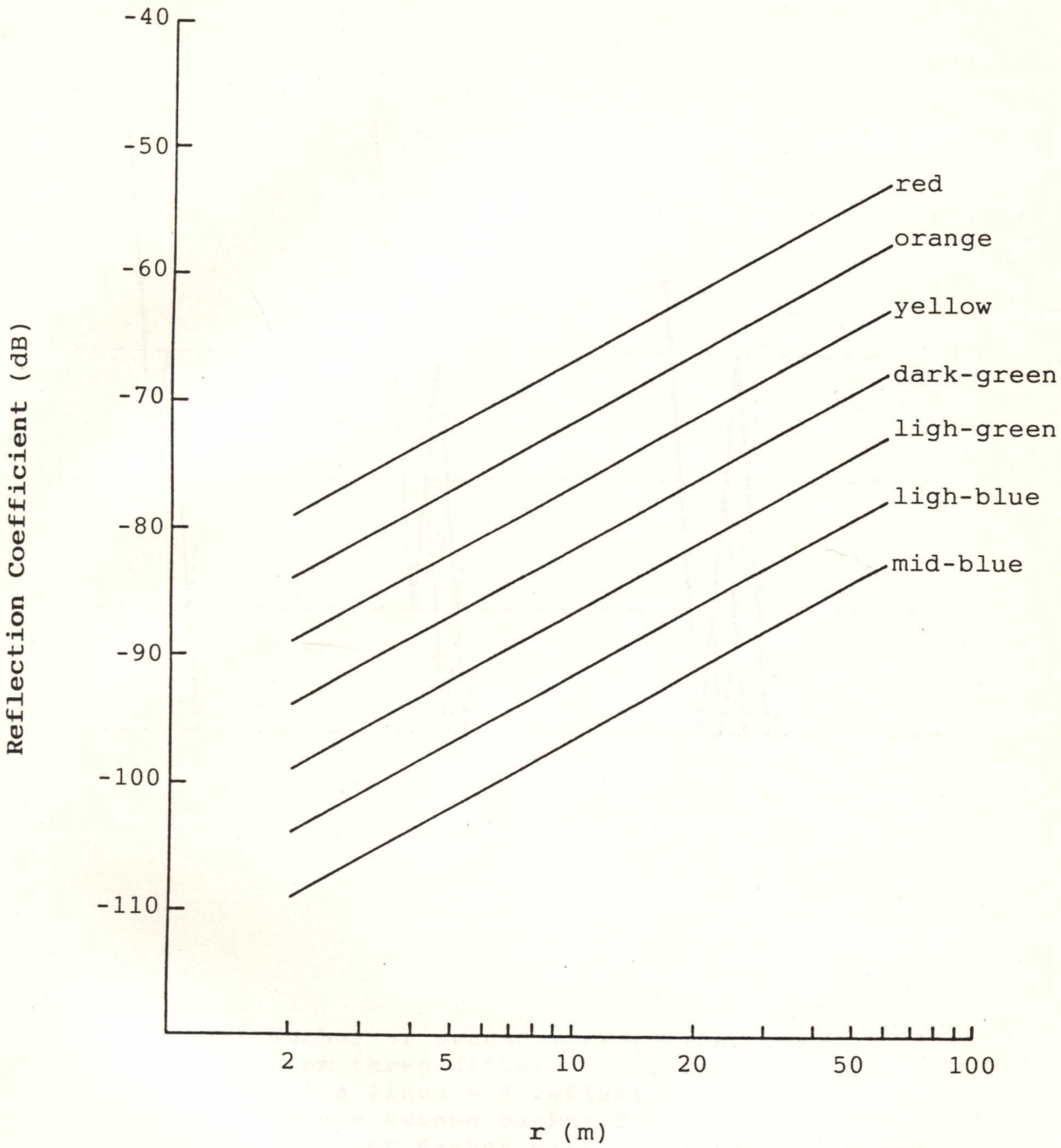

Fig.A5 The relation between the reflection coefficient from a layer of sheet reflectors as a function of range.

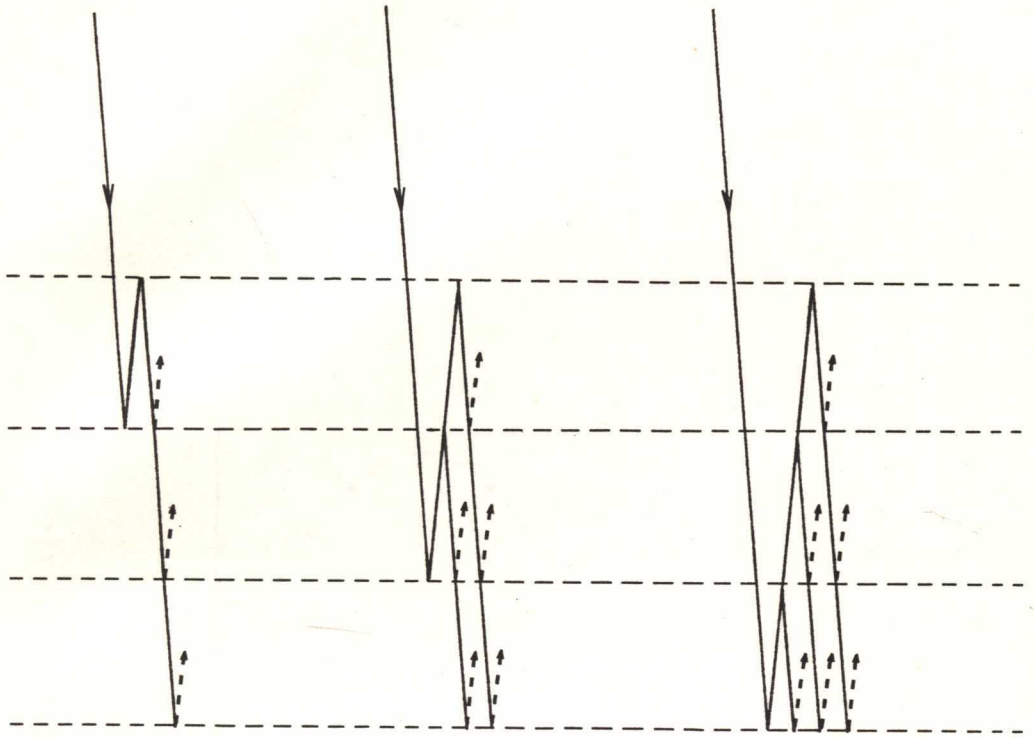

Fig.B1 Number of second back-reflections
from three different layers.
Solid lines are reflection rays
before second back-reflections.
Lines of dashes with an arrow at the end
are the second back-reflection rays.
(Sound is normally incident)

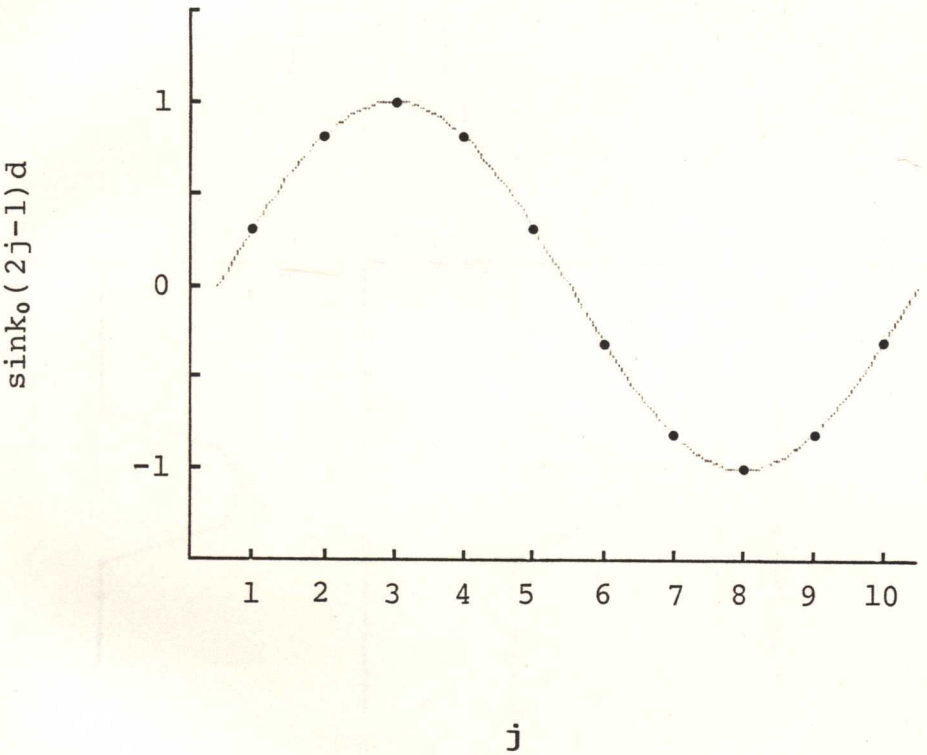

Fig.C1 The imaginary part of the phase of the reflection coefficient, where j is the numerical step number.

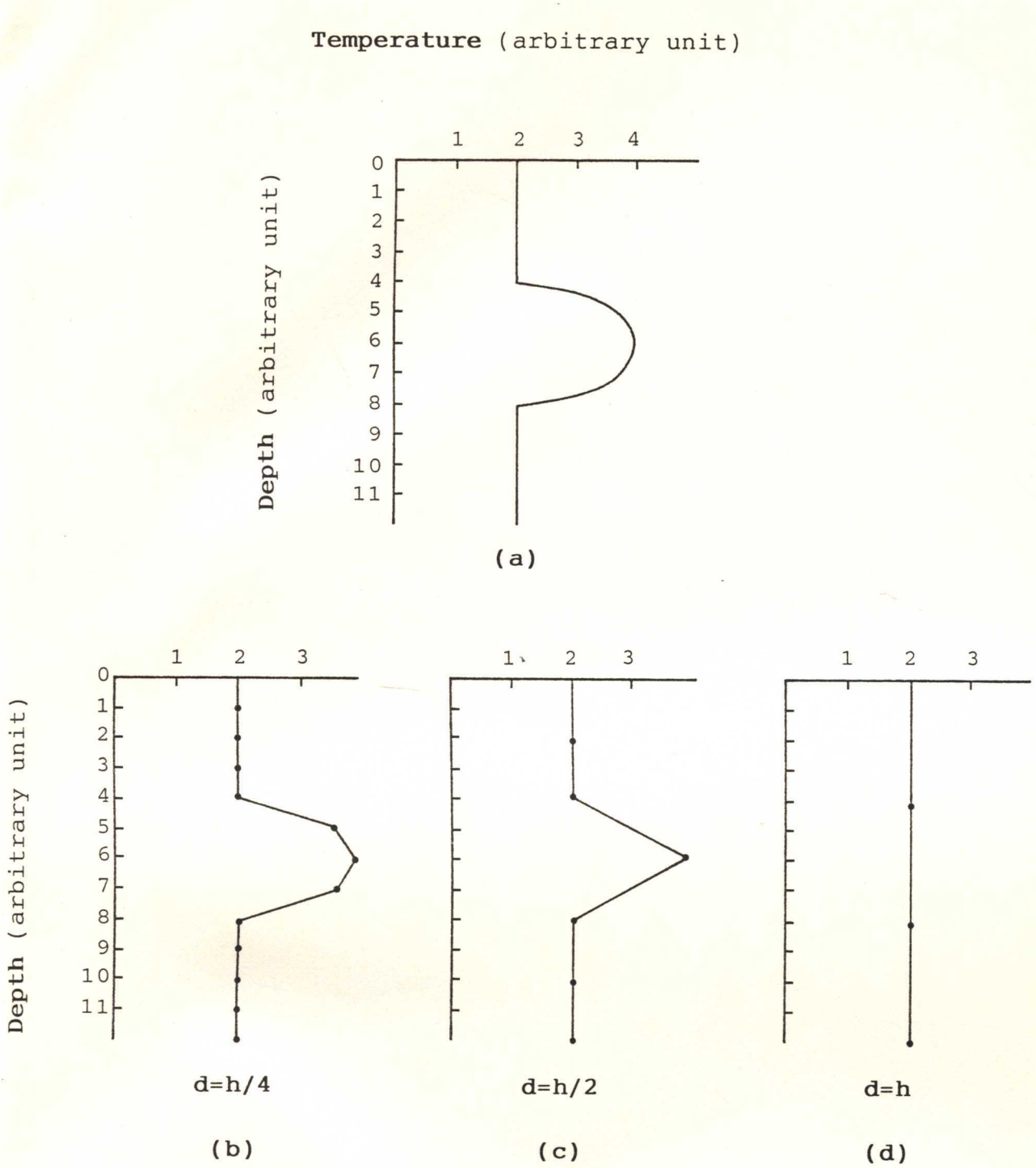

Fig.C2 When sampling separation is not much smaller than the thickness of the layer, error will occur.